Journal of Medicinal Chemistry

Article

pubs.acs.org/jmc

Discovery and Optimization of 1,3,4-Trisubstituted-pyrazolone Derivatives as Novel, Potent, and Nonsteroidal Farnesoid X Receptor (FXR) Selective Antagonists

Huang Huang,[†,∥] Ying Yu,[†,∥] Zhenting Gao,[†] Yong Zhang,[§] Chenjing Li,[‡] Xing Xu,[‡] Hui Jin,[†] Wenzhong Yan,[†] Ruoqun Ma,[†] Jin Zhu,[†] Xu Shen,[†,‡] Hualiang Jiang,[†,‡] Lili Chen,[*,‡] and Jian Li[*,†]

[†]Shanghai Key Laboratory of New Drug Design, School of Pharmacy, East China University of Science and Technology, 130 Mei Long Road, Shanghai 200237, China

[‡]State Key Laboratory of Drug Research, Shanghai Institute of Materia Medica, Chinese Academy of Sciences, 555 Zu Chong Zhi Road, Shanghai 201203, China

[§]Department of Biochemistry, Zunyi Medical College, 201 Dalian Road, Zunyi, Guizhou 563003, China

Supporting Information

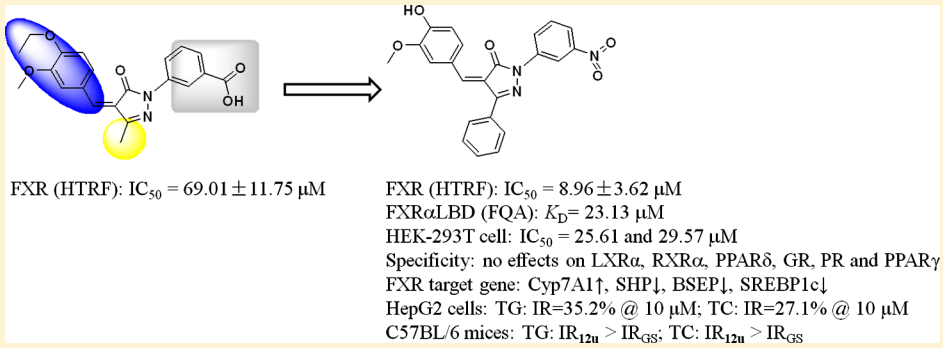

ABSTRACT: LBVS of 12480 in-house compounds, followed by HTRF assay, resulted in one nonsteroidal compound (**11**) with antagonistic activity against FXR (69.01 ± 11.75 μM). On the basis of **11**, 26 new derivatives (**12a–z**) were designed and synthesized accordingly. Five derivatives (**12f–g**, **12p**, **12u**, and **12y**) showed better antagonistic activities against FXR than compound **11**. Remarkably, the most potent derivative, **12u** (8.96 ± 3.62 μM), showed antagonistic capability approximately 10 times and 8-fold higher than that of the control (GS) and the starting compound **11**, respectively. **12u** was further confirmed to have high binding affinity with FXRαLBD, FXR specificity over six other nuclear receptors, and potent antagonistic activity against FXR in two cell testing platforms. **12u** strongly suppressed the regulating effects of CDCA on FXR target genes. The therapeutic potential of **12u** was identified by lowering the contents of triglyceride and cholesterol in human hepatoma HepG2 cells and in the cholesterol-fed C57BL/6 mices.

1. INTRODUCTION

The farnesoid-X-receptor (FXR, NR1H4), a ligand-dependent transcription factor, is a member of metabolic nuclear receptors (NRs) superfamily, highly expressed in liver, intestine, kidney, and other cholesterol-rich tissues such as adrenal glands.[1,2] Cholesterol metabolism end-products, bile acids (BAs), are the major endogenous ligands for FXR, and as an intracellular BA sensor, FXR is the master regulator for bile acid homeostasis.[3] BA-activated FXR mediates hepatoprotection from excess BAs by preventing synthesis and uptake and promoting excretion of BAs: (1) reducing BA synthesis via indirect downregulation of liver-specific cholesterol 7α-hydroxylase (Cyp7A1),[4] a rate-limiting enzyme of the bile acid biosynthetic pathway,[5] (2) reducing the import of BAs from the plasma compartment into the hepatocyte via suppression of Na^+-dependent taurocholate cotransporting polypeptide (NTCP),[6] a hepatic BA import pumps, and (3) increasing the export of BAs out of the hepatocyte into the bile via upregulation of bile salt export pump (BSEP),[7] a hepatic bile acid export pumps.

Apart from its critical role in maintaining bile acid homeostasis, FXR also controls cholesterol, lipid, and glucose metabolism[8,9] and has significant effects on vasculature as well.[10] Furthermore, the roles of FXR have been extended into various other nonmetabolic areas, including liver regeneration[11] and tumorigenesis.[12,13] The results of a growing number of studies suggest that FXR represents an attractive pharmacological target.[9,14−17] However, it is obvious that therapeutically targeting FXR (especially activation) leads to complex responses, some FXR agonists have been found to cause a slight reduction in high-density lipoprotein (HDL) and increased levels of low-density lipoprotein (LDL) in animals

Received: February 27, 2012
Published: August 3, 2012

 © 2012 American Chemical Society

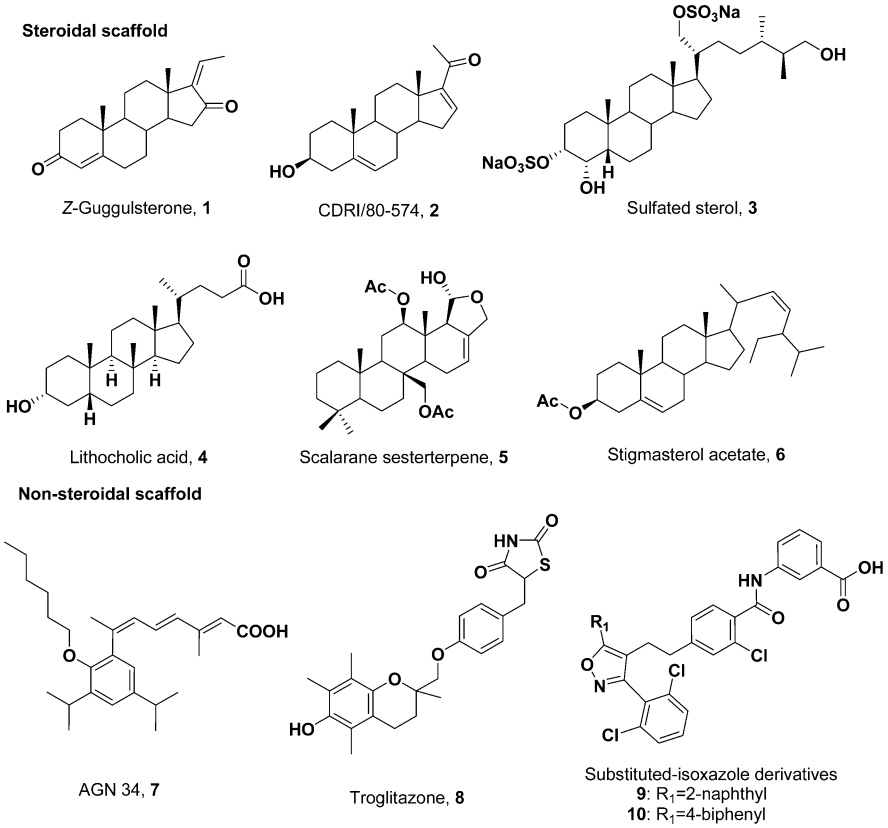

Figure 1. All structures of FXR antagonists reported in literature.

and patients with diabetes and liver steatosis, which might limit FXR agonists development.[18] It would therefore be desirable to develop FXR antagonists that are selective over other NRs (e.g., FXR over liver-X-receptor (LXR)), and we are curious that FXR modulators with such characteristics might have more significant clinical value.

Given the importance of FXR in regulation of numerous biological processes and related disease development, significant efforts have focused on discovering FXR ligands after deorphanization of FXR in 1999.[1] However, survey of the existing FXR ligands reveals that most of the reports deal with FXR agonists and few FXR antagonists have been described so far. FXR antagonists reported have very limited structural diversity and are mainly derived from steroidal scaffold (Figure 1, *Z*-guggulsterone (GS, **1**),[19] CDRI/80−574 (**2**),[20] sulfated sterol (**3**),[21] lithocholic acid (**4**),[22] scalarane sesterterpene (**5**),[23] and stigmasterol acetate (**6**)[24]), and there are only three classes of nonsteroidal scaffold up to now (Figure 1, AGN 34 (**7**),[25] troglitazone (**8**),[26] substituted-isoxazole derivatives (**9**−**10**)[27]). Therefore, clearly seeking potent, structurally novel, nonsteroidal FXR antagonists represents an important direction in the field.

Virtual screening is a well-established tool to identify new lead structures from compound libraries. As the starting point of our efforts on discovering new potential FXR ligands, an in-house library of 12480 compounds was screened using ligand-based virtual screening (LBVS). One nonsteroidal compound (**11**) was identified as an FXR antagonist in homogeneous time-resolved fluorescence assay (HTRF) and selected as the starting point for further structural optimization. Totally, 26 derivatives have been designed, synthesized, and tested with biological assay. Finally, five derivatives (**12f**−**g**, **12p**, **12u** and **12y**) were found to show better antagonistic activities against FXR than the starting compound **11**. In several molecular and cellular assays, the most potent derivative **12u** was identified consistently as a potent and selective FXR antagonist. Furthermore the therapeutic potential of compound **12u** was illustrated by lowering the contents of triglyceride and cholesterol in human hepatoma HepG2 cells (10 μM) and in the cholesterol-fed C57BL/6 mices (oral doses of 50 and 100 mg/kg). Altogether, these data demonstrate that compound **12u** may be a good lead for discovering potential therapeutic drugs for hypercholesterolemia and also be an effective chemical biology tool for the study of FXR-related biological processes and disease.

2. MATERIALS AND METHODS

2.1. Computation. *2.1.1. Virtual Screening.* Before the virtual screening, we searched for known FXR modulators before July 2008 from Thomson Pharma (http://www.thomson-pharma.com/) database and collected 11 FXR modulators, including nine agonists and two antagonists (Supporting Information, Table 1S). Moreover, we selected one more FXR antagonist previously identified in our lab (not published yet). To take advantage of the 12 known modulators, we chose to use ligand-based virtual screening (LBVS) strategy. Schrodinger phase[28] Shape, a ligand-based 3D shape screening tool, was used to screen an in-house compound library (12480 compounds, Figure 2). The 3D structures of the query compounds (12 known modulators) and library compounds were prepared using Schrodinger LigPrep, where the protonation state were assigned with Epik under pH 7. The 3D structures of the library compounds were further calculated by ConfGen Standard Fast mode, with the option "Minimize

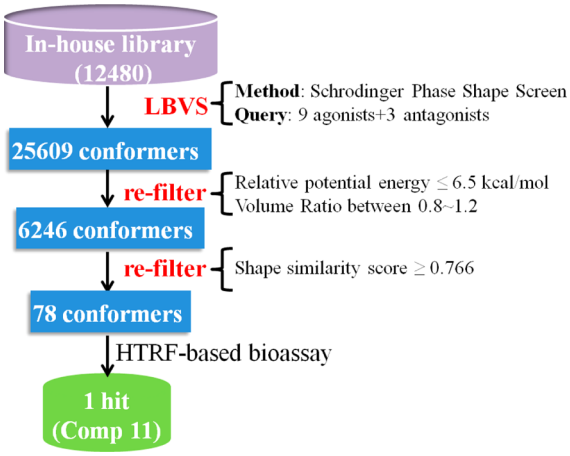

Figure 2. Schematic representation of the virtual screening approach adopted.

the output conformers" enabled, and finally, 290412 structures were generated (about 25 conformers for each library compound). Three key options for phase Shape were modified from default based on our experience: (1) "Volume scoring" was set to "Pharmacophore Types" (this enables the screen to find structural diverse hits with similar pharmacophore features), (2) "Similarity normalization" was set to "Query structure" (this option forces the similarity score to be calculated as the ratio between the overlap volume and the query structure volume), and (3) "Filter out conformers with similarity below" was set to "0.6". The screen yielded 25609 conformers with similarity score higher than 0.6.

The 25609 conformers were further refiltered by three criteria. First, we removed conformers with relative potential energy more than 6.5 kcal/mol to eliminate hit with high strain energy. Second, we calculated the ratio between the molecular volume of the query and library structures and arbitrarily chose the range of 0.8−1.2 as a filter so that library compounds with similar molecular volume to the query compound were kept. After applying above two filters, only 14001 hit conformers were kept. Because each library compound has multiple conformers, only the conformer with highest similarity score was kept, and this further filtered the hits to a total of 6246. Third, we analyzed the distribution of similarity score by plotting a 2D graph of similarity score and rank order (Supporting Information, Figure 1S). In Supporting Information Figure 1S, we noticed a turning point of the curve (similarity score = 0.766), corresponding to the no. 78 hit compound, and the similarity score of other compounds after no. 78 decreases slowly. This means that the bioassay workload will be dramatically increased if similarity score was set to be less than 0.766. So we arbitrarily selected the top 78 conformers (compounds) for bioassay.

2.1.2. Binding Prediction of Compound 11 and 12u. To address the flexibility of FXR binding pocket while predicting ligand−FXR interaction, we included all available crystal structures in the docking model ensemble. Moreover, global strain energy of binding pose was used as a filter to remove unrealistic docking poses (The details see Supporting Information, page S3). Finally, we selected the top scoring pose from the ensemble docking. Only six crystal structures were available when binding model prediction of compound **11** was made in early 2009, but 24 crystal structures were available when binding model prediction of compound **12u** was made in 2012 (Supporting Information, Table 2S).

2.2. Chemistry. Compound **11** (Figure 3) featuring a 4-arylidenepyrazolone framework was obtained from the in-house

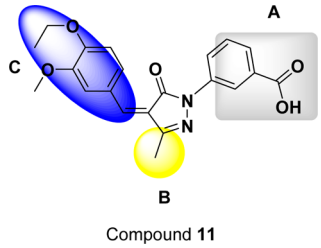

Figure 3. Structure and three chemical modification regions of compound **11**.

compound library by virtual screening and selected for designing new FXR antagonists. We have previously developed a simple, rapid, and efficient one-pot protocol for the preparation of the 4-arylidenepyrazolone derivatives by solvent-free microwave-assisted reaction.[29] Furthermore, the versatility of this methodology is suitable for 1,3,4-trisubstituted-pyrazolone library synthesis from commercially available starting materials. With the aid of the predicted interactions between **11** and the FXR active site (see section 3.5. Binding Models), considering the 1,3,4-substitution patterns accessibility of compound **11**, we started from keeping the common moiety (pyrazolone framework), and modified three regions of this molecule to get some structure−activity relationship (SAR) information and improve antagonistic activity: (A) replacing the 3′-carbonyl substituted phenyl in region A with different electronic and hydrophobic substituted phenyls (**12a−b**, **12h**, and **12j−z**) to determine if the hydrogen bond interaction between residue Arg331 and carbonyl substituent (see Figure 12A,B) is necessary for ligand−receptor interaction, (B) changing the methyl group in region B with bulky phenyl (**12u**) and isopropyl (**12v**) groups, respectively, to explore if enough spatial volume within the binding pocket of the receptor around the methyl group of compound **11** is available to accommodate large chemical moieties (see Figure 12C,D), and (C) examples of variations in region C include different substitutions on the phenyl portions (**12a**, **12c−g**, **12i**, **12u−v**, and **12x−z**), changing the phenyl into heterocycle (**12w**) and naphthalenyl (**12t**), changing the hydrogen atom into methyl (**12x**), and changing ene linker into diene linker (**12i**). We hope to determine if 4-arylidene moiety can be extended to capture more interactions and the type of 4-arylidene moiety would affect antagonistic activity (Figure 3).

On the basis of the above design, compounds **11**, **12a−g**, and **12j−y** were synthesized through the route outlined in Scheme 1 by employing our previous method.[29] Various β-ketoesters, hydrazines, and aldehydes or ketones were placed in a domestic microwave oven and irradiated at a power of 420 W for 10 min to afford target products in good to excellent yields.

Scheme 2 depicts the sequence of reactions that led to the preparation of compounds **12h−i** using 3-hydrazinylbenzoic acid **15a** as the starting material. Refluxing **15a** in ethanol catalyzed with conc H_2SO_4 afforded compound **16**, which was condensed with ethyl acetoacetate to afford pyrazolone **17**. Compounds **12h** and **18** were prepared by condensing **17** with aldehydes **13a** and cinnamaldehyde, repectively, under

Scheme 1[a]

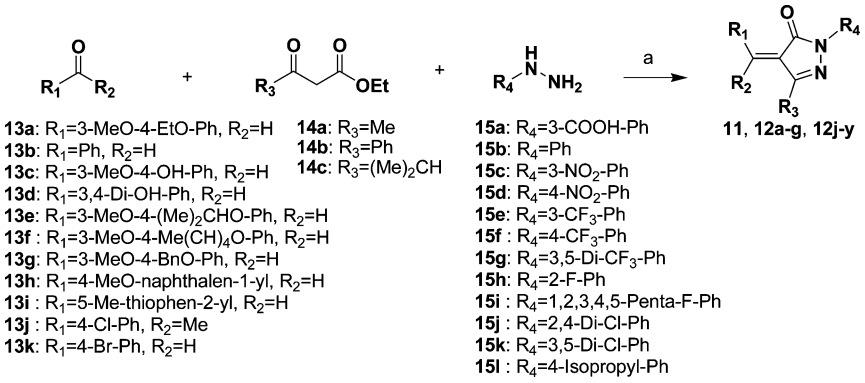

[a]Reagents and conditions: (a) MWI, 420 w, 10 min.

Scheme 2[a]

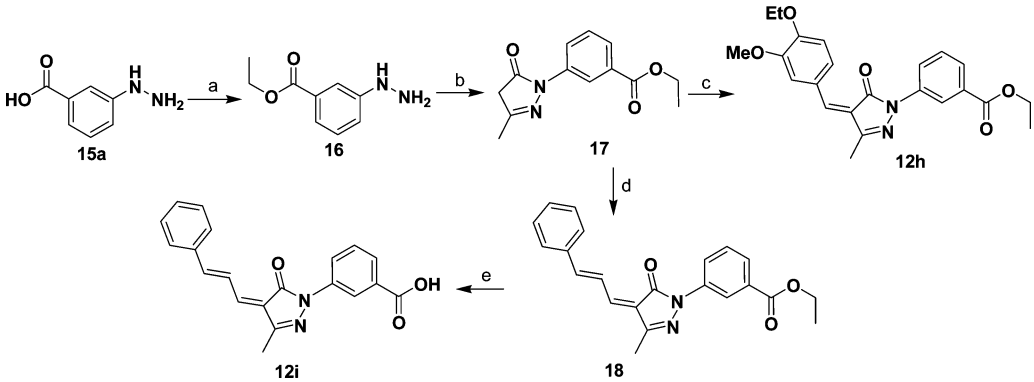

[a]Reagents and conditions: (a) EtOH, concd H_2SO_4, reflux, overnight; (b) AcOH, ethyl acetoacetate, reflux, 4 h; (c) **13a**, 130 °C, 30 min; (d) cinnamaldehyde, 130 °C, 30 min; (e) EtOH:THF:H_2O = 3:3:1, LiOH, rt 8 h.

Knoevenagel reaction condition. Compound **12i** was obtained by hydrolysis of **18** using LiOH at room temperature.

Compound **12z** was prepared from compound **12c** by selective esterification with 2-bromopropane (Scheme 3). All chemical structures of compounds **11** and **12a−z** were listed in Table 1.

Scheme 3[a]

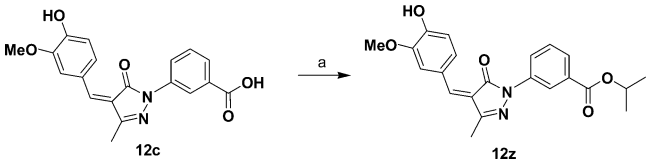

[a]Reagents and conditions: (a) (i) DMF, K_2CO_3, reflux 30 min; (ii) Me_2CHBr, 60 °C, 8 h.

2.3. Biological Assay. *2.3.1. Protein Expression and Purification.* The coding region of human FXRαLBD (residues 238−473) was cloned into the vector pGEX 6P-1(Amersham) or pET-15b (Invitrogen). *Escherichia coli* BL21 (DE3) cells (Promega) were transformed with the above plasmids and cultivated at 37 °C in LB medium. The culture was induced with 0.2 mM IPTG and incubated at 20 °C for 6 h. GST-tagged FXRαLBD or His-tagged FXRαLBD was purified with Glutathione-Sepharose 4B resin (GE Healthcare) or Ni-NTA resin (Qiagen), respectively. The proteins were further purified with Superdex 75 (Amersham Pharmacia Biotech). The purified proteins were dialysized against the suitable buffers and immediately stored at −80 °C for later use. GST-tagged FXRαLBD was used in HTRF, and FXRαLBD was used in fluorescence quenching assay.

2.3.2. HTRF Assay. HTRF assay was carried out as previously described with some modifications.[19] Biotinylated SRC1 peptide (5′-biotin-CPSSHSSLTERHKILHRLLQEGSPS-$CONH_2$) was synthesized by Shanghai Shengong Biotechonology (Shanghai, China). The experiment was performed by incubating 10 nM GST-FXRαLBD, 0.83 nM anti-GST-(Eu) K, 100 nM biotin-SRC,1 and 41.75 nM SA/XL665 in assay buffer (50 mM Hepes, pH7.0, 125 mM KF, pH7.0, 0.125% CHAPS, 0.05% dry milk) in the presence of test compounds or coincubating with chenodeoxycholic acid (CDCA) for 30 min at room temperature. Data were collected using a SpectraMax M5 microplate reader (Molecular Devices, Sunnyvale, CA) and calculated using the equation 1000 × (668 nm/620 nm).

2.3.3. Fluorescence Quenching Assay. Fluorescence spectra were measured according to the previously published approach.[30] Briefly, FXRαLBD protein was purified using Ni-NTA resin and ion exchange chromatography after the removal of His-tag with thrombin (Sigma). Purified FXRαLBD protein was incubated with different concentrations of the test compound at 4 °C for 1 h. Protein quenching was monitored using a HITACHI fluorescence spectrophotometer (F-4500, HITACHI) at 25 °C with 5 nm of excitation and 5 nm of emission slit-width. The excitation wavelength was 280 nm and

Table 1. Chemical Structures of Compounds 11, 12a−z, and Their Activities Based on HTRF

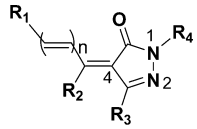

Cmpd	R_1	R_2	R_3	R_4	n	agonistic rate at 40 μM (%)	antagonistic rate at 40 μM (%)	IC_{50}[a] (μM)
11	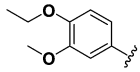	H	Me	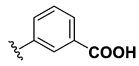	0	9.0	48.5	69.01±11.75
12a		H	Me		0	<5	23.1	
12b	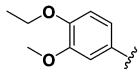	H	Me		0	<5	26.0	
12c	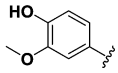	H	Me	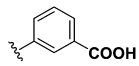	0	6.4	<5	
12d	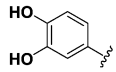	H	Me	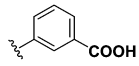	0	<5	17.4	
12e	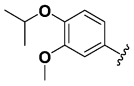	H	Me	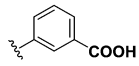	0	<5	<5	
12f	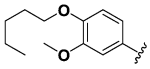	H	Me	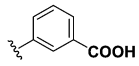	0	<5	55.4	39.16±5.44
12g	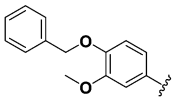	H	Me	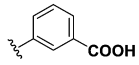	0	<5	57.5	33.83±4.77
12h	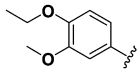	H	Me	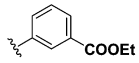	0	<5	9.4	
12i		H	Me	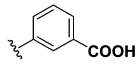	1	<5	32.1	
12j	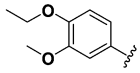	H	Me	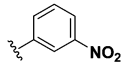	0	29.2	<5	
12k	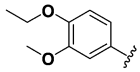	H	Me	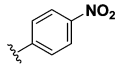	0	12.7	14.8	
12l	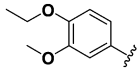	H	Me	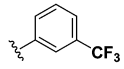	0	<5	<5	
12m	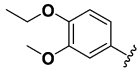	H	Me	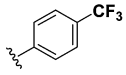	0	<5	9.5	
12n	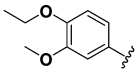	H	Me	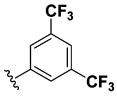	0	<5	<5	
12o	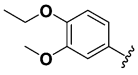	H	Me		0	<5	5.5	

dx.doi.org/10.1021/jm3002718 | J. Med. Chem. 2012, 55, 7037−7053

Table 1. continued

Cmpd	R_1	R_2	R_3	R_4	n	agonistic rate at 40 μM (%)	antagonistic rate at 40 μM (%)	IC_{50}[a] (μM)
12p	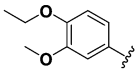	H	Me	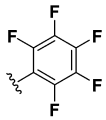	0	<5	43.6	82.20±12.20
12q	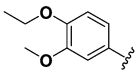	H	Me	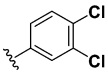	0	<5	7.3	
12r	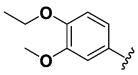	H	Me	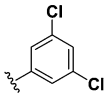	0	<5	<5	
12s	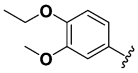	H	Me	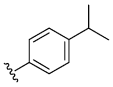	0	<5	7.7	
12t	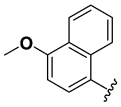	H	Me	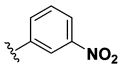	0	<5	22.7	
12u	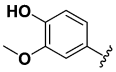	H	Ph	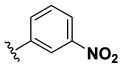	0	<5	70.4	8.96±3.62
12v	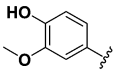	H	$(Me)_2CH$	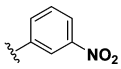	0	<5	26.4	
12w		H	Me	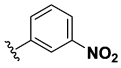	0	<5	<5	
12x	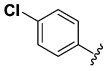	Me	Me	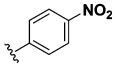	0	<5	16.8	
12y	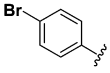	H	Me		0	<5	72.6	9.93±1.14
12z	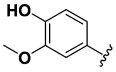	H	Me	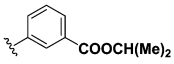	0	<5	29.9	

[a]Control assays were performed with CDCA (FXRα agonist) or CDCA plus GS (FXRα antagonist). EC_{50} of CDCA and IC_{50} of GS were determined with the values of 12.5 and 89.36 μM, respectively. Values are presented as the means ± SE of three independent experiments.

the emission spectra were measured between 300 and 400 nm. The binding affinity (K_D) of test compound to FXRαLBD protein was fitted as the previously reported method.[30]

2.3.4. Differential Scanning Calorimetry (DSC) Assay. DSC experiments were performed using a Microcal VP-Capillary DSC instrument (Microcal, Amherst, MA). FXRαLBD protein was dialyzed to equilibrium against 20 mM Tris-HCl, 50 mM NaCl, pH 8.0, and the dialysis reservoir was served as the reference buffer. Two mg/mL FXRαLBD protein with dimethyl sulfoxide (DMSO) or the compound was used as the sample. Temperatures from 10 to 110 °C were scanned at a rate of 90 °C/h. The data were analyzed with ORIGIN software (Microcal).

2.3.5. Luciferase Reporter Assay. Mammalian one-hybrid and transactivation experiment were performed as previously described method.[31] HEK293T cells were cultured in 24-well plate. In mammalian one-hybrid assay, ligand-binding domain of different nuclear receptor was fused to Gal4 DNA binding domain. The fusion construct and UAS-luciferase reporter vector were transiently into the cells. In the transactivation experiment, HEK293T cells were transiently transfected with pcDNA3.1-FXRα, pcDNA3.1-retinoid-X-receptor α (RXRα), pGL3- FXR response element(FXRE)-Luc, and *Renilla* luciferase vector pRL-SV40. After 6 h, the transfection mixture was replenished with fresh medium containing the test compounds. Luciferase activities were determined using a Dual-Luciferase Assay System (Promega, USA) strictly according to the manufacturer's instructions.

2.3.6. Quantitative Real-Time Polymerase Chain Reaction (RT-PCR) Analysis. Quantization of the expression level of FXR target genes was performed by quantitative RT-PCR. HepG2 cells were cultured in 6-well plate and incubated with different concentrations of test compounds for 24 h. Total RNA was isolated with TRIzol reagent (TaKaRa, Japan). Complementary cDNA was synthesized according to the protocol of PrimeScriptTM RT reagent Kit (TaKaRa, Japan). Real-time PCR was carried out using SYBR Green Real-time PCR master mix (TaKaRa, Japan) using DNA Engine Opticon 2 System (Bio-Rad Laboratories, USA). Sequences of all the primers are listed in Table 2. The relative objective mRNA levels were

Table 2. The Sequences of All the Primers in Quantitative RT-PCR Analysis

genes	forward primer[a]	reverse primer[a]
SHP	CACTGGGTGCTGTGTGAAGT	TAGGGCGAAAGAAGAGGTCCC
CYP7A1	GAGAAGGCAAACGGGTGAAC	GCACAACACCTTATGGTATGACA
SREBP1-c	ACTTCCCTGGCCTATTTGACC	GGCATGGACGGGTACATCTT
BSEP	CAGGCGTGCTACTCATTTTTGG	AACCCACAACGTGTTCCATTT
β-actin	CATGTACGTTGCTATCCAGGC	CTCCTTAATGTCACGCACGAT

[a]All are *Homo sapiens* primers.

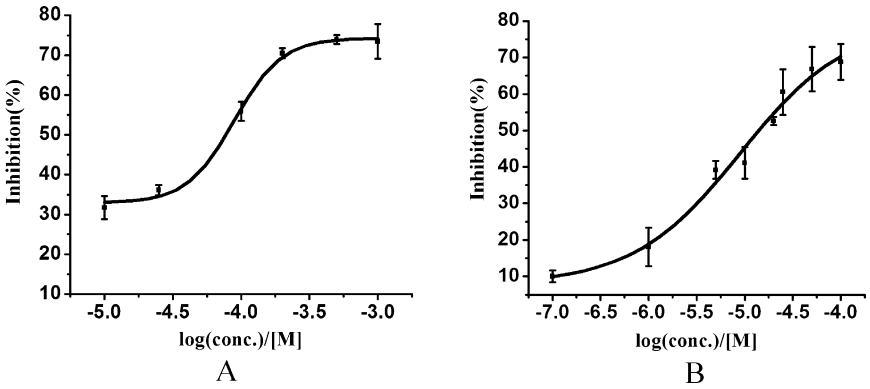

Figure 4. GS (A) and compound **12u** (B) inhibit the effect of CDCA by HTRF method.

calculated as a ratio to those of β-actin, respectively. Data was determined in triplicate experiments.

2.3.7. Determination of Triglyceride and Cholesterol Contents. HepG2 cells cultured in 6-well plates were starved overnight with the fresh DMEM without FBS and then treated with vehicle (DMSO) or tested compound for another 24 h with DMEM without FBS. Finally, cells were lysed in RIPA buffer (25 mM Tris-HCl, pH 7.6, 150 mM NaCl, 1% NP-40, 1% sodium deoxycholate, 0.1% SDS) (Thermo Scientific, USA) for 30 min and sonicated on ice. The suspension was centrifuged for 30 min at 12000 rpm at 4 °C. The middle clear layers were used to further determine the content of the total protein, triglyceride, and cholesterol. Total protein was determined using BCA (bicinchoninic acid) Protein Assay Reagent Kit (Thermo Scientific, USA). Triglyceride and total cholesterol contents were measured by use of the kits (Nanjing Jiancheng Bioengineering Institute, Nanjing, China).

2.3.8. Pharmacological Studies. All procedures performed on animals were conducted in strict accordance with the ethical guidelines of Animal Care and Use Committee (Shanghai Institute of Materia Medica, Chinese Academy of Sciences). The pharmacological studies of compound **12u** were carried out according to the previous reported method.[19] Male 8−12-week-old C57BL/6 mice (Shanghai SLAC Laboratory Animal Co. Ltd.) were randomly divided into five groups with nine animals per group. Animals in the control group were fed a ground-chow diet (Shanghai SLAC Laboratory Animal Co. Ltd.), and the other four groups were fed a ground-chow diet containing 2% content of cholesterol (Shanghai SLAC Laboratory Animal Co. Ltd.). GS (100 mg/kg) and compound **12u** (50 and 100 mg/kg) were resuspended in 0.5% CMC-Na and administered to animals by oral gavage. Control and vehicle animals received the same amount of 0.5% CMC-Na. At the end of 10-day treatment, animals were sacrificed after an overnight fast. Blood and liver samples were collected for further determining the cholesterol and triglyceride levels.

2.3.9. Statistical Analysis. All the experiments were performed at least three times. Results were presented as mean ± standard error (SE). Differences between groups were analyzed for statistical significance using Student's *t* test. *P* values of 0.001, 0.01, and 0.05 were considered statistically significant.

3. RESULTS AND DISCUSSION

3.1. Identification of the Lead Compound 11 by Virtual Screening. Targeting the 3D structure of 12 query compounds (nine agonists and three antagonists), we searched the in-house compound library by using Schrodinger phase (LBVS). The final list consists of 78 candidates for biological assay. To quickly identify the active compound, we first investigated the agonistic or antagonistic (hits plus CDCA) activities of these 78 compounds against FXR using HTRF-based assay. One hit (compound **11**, Figure 3) ranked as no. 57 from the LBVS candidates was found to be FXR antagonist (IC_{50} = 69.0 ± 11.8 μM, Table 1). Compound **11** is most similar to the antagonist previously identified in our lab (unpublished data), with a similarity score of 0.768. Compound **11** is larger than our in-house identified antagonist, and the molecular volume ratio between two compounds is 1.12 (Supporting Information, Figure 2S).

3.2. Derivatives Design and Synthesis. Totally, 27 compounds (**11** and **12a−z**) were designed and synthesized, and their chemical structures are shown in Table 1. These compounds were synthesized through the routes outlined in Schemes 1−3, and the details for synthetic procedures and structural characterizations are described in the Experimental Section. All compounds (**11** and **12a−z**) were confirmed ≥95% purity (Supporting Information, Table 3S).

3.3. Biological Activities. *3.3.1. Agonistic and Antagonistic Activities of Derivatives **12a−z**.* For the primary assay, the percent agonistic and antagonistic activities of the derivatives **12a−z** at 40 μM were measured using HTRF-based FXR coactivator association assay. The results are

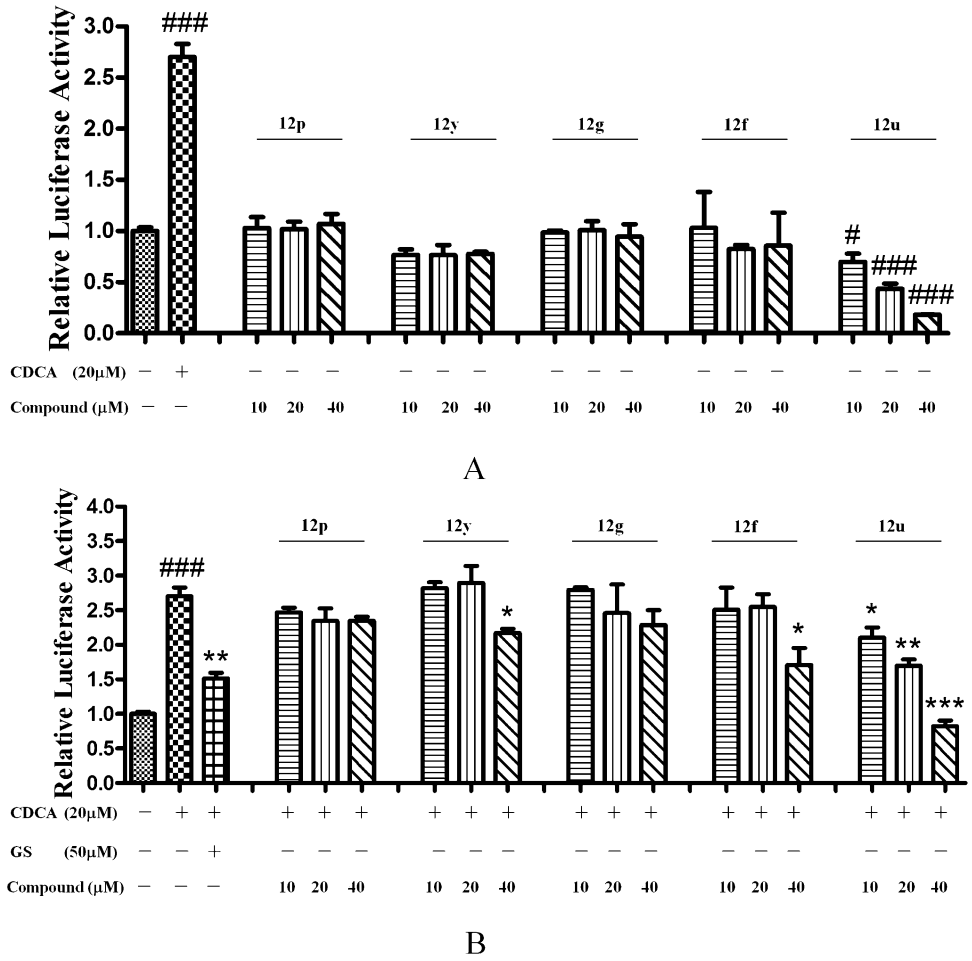

Figure 5. Agonistic and antagonistic activities of 5 compounds (**12f–g**, **12p**, **12u**, and **12y**) in the transactivation assay. HEK-293T cells were transiently transfected with pcDNA3.1-FXRα, pcDNA3.1-RXRα, pGL3-FXRE, and pRL-SV40 plasmids. Cells were treated with varied concentrations of compounds in the absence or presence of CDCA (20 μM) for 18 h. FXRα antagonist GS was used as a control. Values are presented as the means ± SE of three independent experiments. (A) ### $P < 0.001$, *$P < 0.05$, **$P < 0.01$, and ***$P < 0.001$ vs DMSO, respectively. (B) ### $P < 0.001$ vs DMSO; *$P < 0.05$, **$P < 0.01$, and ***$P < 0.001$ vs 20 μM CDCA.

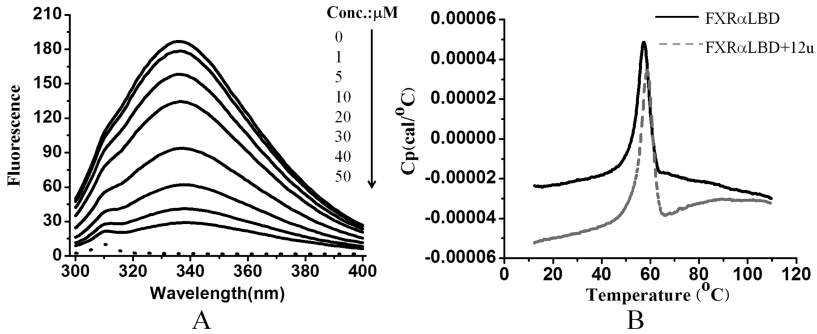

Figure 6. Compound **12u** physically binds to FXRαLBD. (A) Fluorescence spectra of different concentrartions of **12u** and FXRαLBD (solid line). The fluorecence spectra of 50 μM **12u** was shown as the dashed line. (B) Thermal stabilities of FXRαLBD and the complex of FXRαLBD/**12u**. The concentration of FXRαLBD was 2 mg/mL ($C_{12u}/C_{FXR\alpha LBD}$ = 5/1).

summarized in Table 1. Of the synthetic derivatives tested, almost all derivatives have no agonistic activities (expressed as agonistic rate at 40 μM < 10%), only two derivatives (**12j–k**, Table 1) show little agonistic activities. Encouragingly, five derivatives (eg., **12f–g**, **12p**, **12u**, and **12y**) displayed good antagonistic activities against FXR (expressed as antagonistic rate at 40 μM ≥ 40%), indicating that these are good candidate antagonists of FXR. Therefore, we determined their IC_{50} values, which are, respectively, 39.16 ± 5.44, 33.83 ± 4.77, 82.20 ± 12.20, 8.96 ± 3.62, and 9.93 ± 1.14 μM (Table 1). GS was used as the positive antagonist. As indicated in Figure 4A,B, GS (IC_{50} = 89.36 μM, Figure 4A) and the most potent compound **12u** (Figure 4B) dose-dependently inhibited the effect of CDCA induced the interaction between FXR and the coactivator SRC-1.

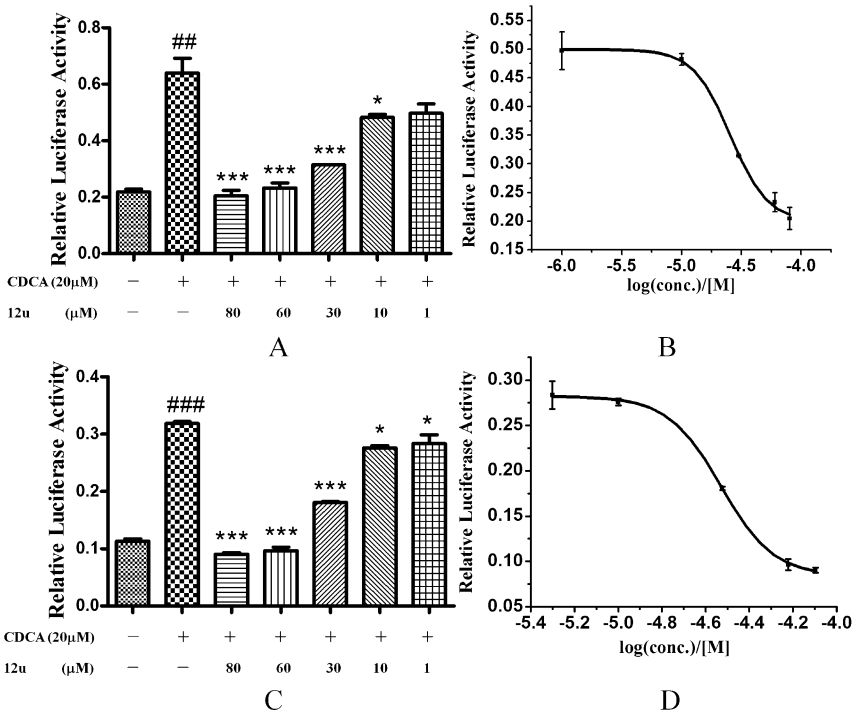

Figure 7. The antagonistic activities of compound **12u** by the mammalian one-hybrid (A−B) and transactivation experiment (C−D). Values are presented as the means ± SE of three independent experiments. ##P < 0.01 and ###P < 0.001 vs DMSO; *P < 0.05 and ***P < 0.001 vs 20 μM CDCA.

As we have known, FXRα have to form FXRα:RXRα heterodimer with RXRα and then bind to their response element FXRE to regulate the downstream genes expression. We thus further evaluated the effects of five antagonists against FXR using transactivation assay. As indicated in Figure 5A,B, 20 μM CDCA induced about 2.6-fold increase of luciferase activity, which was completely abolished by the treatment of 50 μM GS, indicating the reliability of our platform. Of all five antagonists, none of these compounds appear to be an FXR agonist in the transactivation assay (Figure 5A), however, compound **12u** could cause a significant inhibition of FXR transactivation induced by CDCA in a dose-dependent manner and completely reverse the effect exerted by CDCA on FXR transactivation at a concentration of 40 μM (Figure 5B, ***P < 0.001 vs CDCA alone).

*3.3.2. Compound **12u** Physically Binds to FXRαLBD.* The luciferase assay indicated that compound **12u** exhibited strong antagonistic activity on FXR transcription. We thus tested the binding affinity of compound **12u** to FXR with two methods. First, we determined the physical interaction between compound **12u** and FXRαLBD by fluorescence quenching analysis. As shown in Figure 6A, FXRαLBD displayed maximal fluorescence at 337 nm, whereas compound **12u** itself had no fluorescence at this wavelength. When 1 μM FXRαLBD was incubated with increasing amounts of compound **12u**, the fluorescence intensity was quenched in a dose-dependent manner. Their association constant (K_D= 23.13 μM) were fitted according to the previous method.[30] In addition, we performed the differential scanning calorimetry assay to determine the thermodynamic stability of FXRαLBD in the presence or absence of compound **12u**, DSC curves were shown in Figure 6B. When compound **12u** was incubated with FXRαLBD protein, the T_m value increased from 57.33 to 58.74 °C. This result thereby suggested that compound **12u** as FXR ligand could bind to FXRαLBD and also increase the thermal stability of FXRαLBD protein.

*3.3.3. Compound **12u** Inhibits the Effect of CDCA.* To further determine the cellular effects of compound **12u** as the FXR antagonist, we performed the mammalian one-hybrid and transactivation assay, respectively. In the mammalian one-hybrid assay, HEK-293T cells were transiently cotransfected with pCMX-Gal4DBD-FXRαLBD fusion vector, UAS-TK-Luc reporter, and *Renilla* luciferase vector pRL-SV40. The transfected cells were then incubated with vehicle, compound **12u**, for 18 h with or without 20 μM CDCA. As shown in Figures 7A,B, 20 μM CDCA stimulated about 3-fold increase of luciferase activity, which was completely abolished by the treatment of 60 μM compound **12u**, while the similar antagonistic activity was also detected in transactivation assay (Figures 7C,D). The IC_{50} values were 25.61 and 29.57 μM in both testing platforms, respectively, which is in good accordance to the binding affinity between compound **12u** and FXRαLBD in molecular level (Section 3.3.2).

*3.3.4. Compound **12u** is a FXR Selective Antagonist.* To further investigate the specificity of compound **12u**, we thus tested the interactions of compound **12u** and other nuclear receptors including RXRα, LXRα, GR, PR, PPARδ, and PPARγ according to the published method (Figure 8).[32] The results showed that compound **12u** (20 μM) had no agonistic (**12u** alone) or antagonistic (**12u** plus the corresponding agonists) effects on RXRα (A), LXRα (B), GR (C), PR (D), PPARδ (E), but it exhibited weak PPARγ-agonistic activity (<15.2%) (F). These results suggested, to a certain extent, that compound **12u** might be a selective antagonist of FXR.

*3.3.5. Compound **12u** iInhibits Transcription of FXR Downstream Genes.* To gain further insights into the antagonistic activity of compound **12u**, we then investigated the downstream genes of FXR by RT-PCR method. The cells

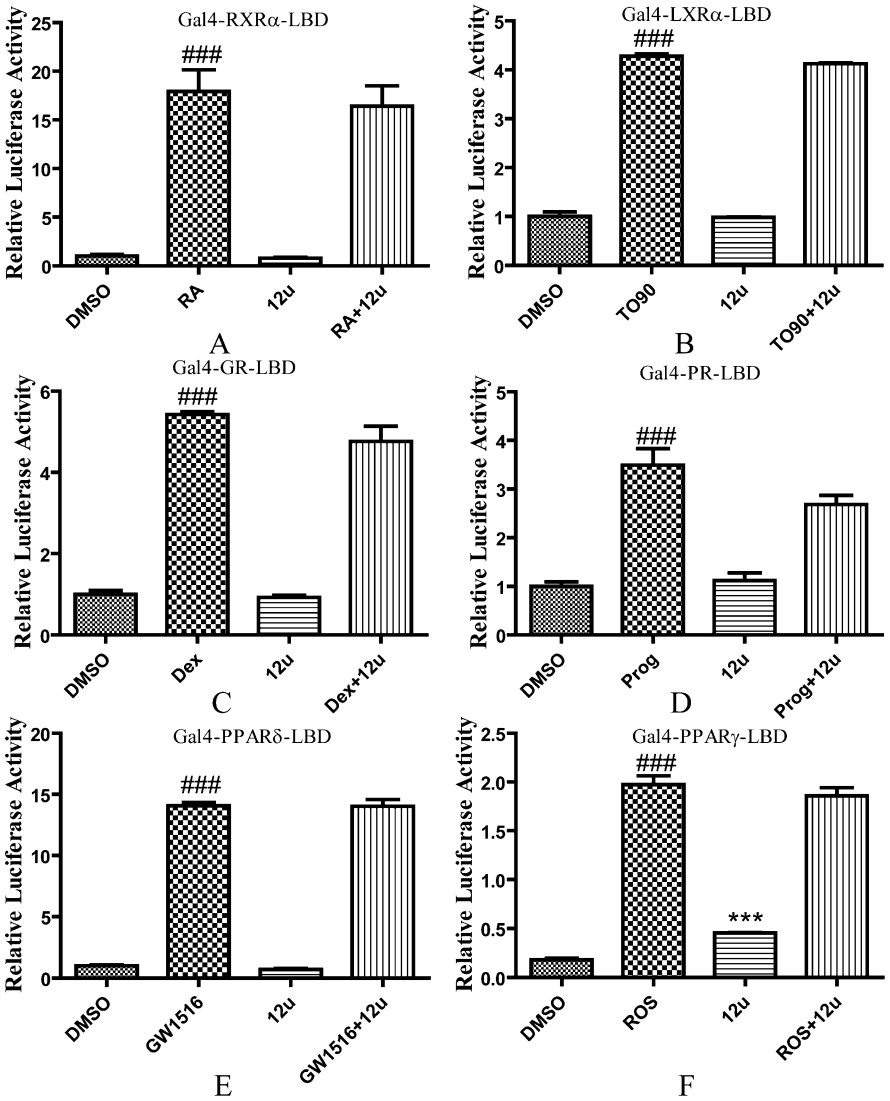

Figure 8. Specificity of compound **12u** was performed by the mammalian one-hybrid assay. HEK-293T cells were transiently cotransfected with the fusion plasmid of Gal4 DBD-NR-LBD, including RXRα (A), LXRα (B), GR (C), PR (D), PPARδ (E), and PPARγ (F) in combination with the UAS-TK-Luc reporter. RXRα agonist 9*c*RA (RA, 0.1 μM), LXRα agonist TO901317 (TO90, 0.5 μM), GR agonist dexamethasone (Dex, 50 nM), PR agonist progesterone (Prog, 100 nM), PPARδ agonist GW1516 (GW1516, 10 μM), and PPARγ agonist rosiglitazone (ROS, 10 μM) were as the positive controls. Values are presented as the means ± SE of three independent experiments. *$P < 0.05$ vs agonist; #$P < 0.05$ and ###$P < 0.001$ vs DMSO.

cultured in 6-well plates were treated with DMSO and different concentrations of compound **12u** in the presence or absence of CDCA. After a 24 h treatment, cells were collected for RT-PCR analysis. As indicated in Figure 9, CDCA could inhibit the expression of canonical FXR target gene Cyp7A1 (A) but induce the expression of small heterodimer partner (SHP) (B), BSEP (C), and sterol regulatory element-binding protein 1c (SREBP1c) (D). Interestingly, compound **12u** strongly suppressed the effect of CDCA. Altogether, these data thus indicate that we have identified compound **12u** as a potent and selective FXR antagonist.

*3.3.6. Compound **12u** Efficiently Lowers Triglyceride and Cholesterol Contents.* As reported, FXR antagonist GS could decrease hepatic cholesterol levels in the cholesterol-fed wild-type animals.[19] To investigate whether compound **12u** also influences lipid metabolism, we tested its lipid-lowering activities in human hepatoma HepG2 cells. HepG2 cells in a 6-well plate were treated with DMSO, GS, or different concentrations of compound **12u** for 24 h and then the level of the lipids was determined. As shown in Figure 10, 10 μM compound **12u** decreased the contents of triglyceride (35.2%, A) and cholesterol (27.1%, B) dose-dependently, with a similar potency to that of 40 μM GS (TG, 39.8%; TC, 25.2%). These results are in good accordance to effects on the expression of genes of compound **12u** (Section 3.3.5). Compound **12u** could downregulate SREPB1c expression induced by CDCA in HepG2 cells (Figure 9D). SREPB1c was a master gene regulator that increases liver expression or activity of many genes involved in fatty acids and trygleride synthesis such as acetyl-CoA carboxylase (ACC), acetyl-CoA synthetase (AceCS), and fatty acid synthase (FAS).[33] Inhibition of SREPB-1c by compound **12u** might be responsible for the lowering triglyceride effect in HepG2 cells (Figure 10A). Considering Cyp7A1's critical role in accelerating cholesterol degradation, the upregulated expression of Cyp7A1 induced by

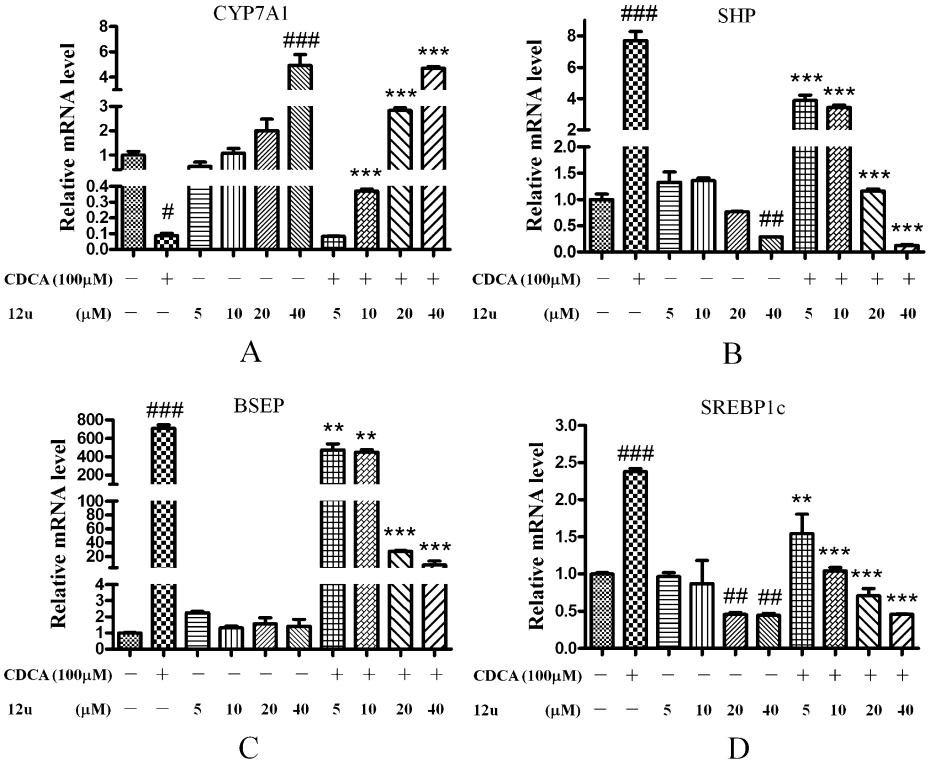

Figure 9. Compound **12u** inhibits transcription of FXR downstream genes. HepG2 cells cultured in 6-well plate were treated with DMSO and different concentrations of compound **12u** with or without 100 μM CDCA for 24 h. The treated cells were collected for RT-PCR analysis. The mRNA levels of Cyp7A1 (A), SHP (B), BSEP (C), and SREBP1c (D). Their relative changes were normalized to β-actin level. Values are presented as the means ± SE of three independent experiments. #P < 0.05, ##P < 0.01, and ###P < 0.001 vs DMSO; *P < 0.05, **P < 0.01, and ***P < 0.001 vs 100 μM CDCA.

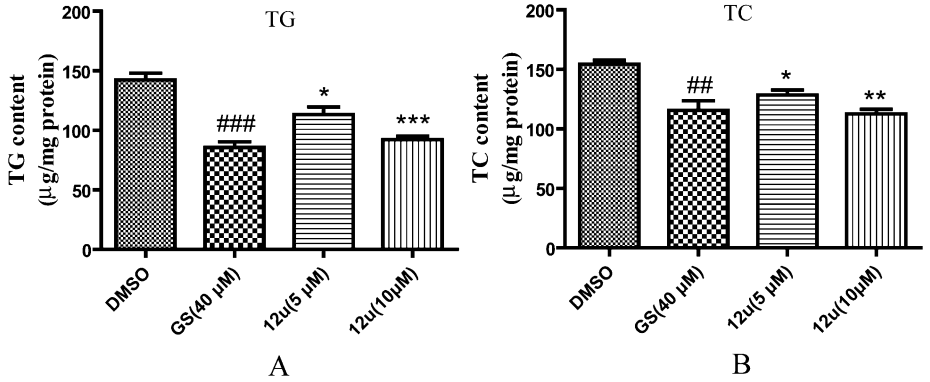

Figure 10. Compound **12u** efficiently decreases triglyceride (A) and cholesterol (B) contents dose-dependently. HepG2 cells were starved in serum-free medium overnight and treated with different doses of compound **12u** or 40 μM GS as the positive control for 24 h before the experiments. ##P < 0.01 and ###P < 0.001 vs DMSO; *P < 0.05, **P < 0.01, and ***P < 0.001 vs DMSO.

compound **12u** (Figure 9A) could be a reason why the content of cholesterol in HepG2 cells were lowered (Figure 10B).

Similarly, an in vivo pharmacological evaluation also showed that compound **12u** could effectively lower serum and hepatic triglyceride and total cholesterol in the cholesterol-fed C57BL/6 mices (Figure 11). Compound **12u** significantly decreased the levels of serum triglycerides dose-dependently with the reduction of 48.4 and 60.3% at dosages of 50 and 100 mg/kg, respectively, compared with the vehicle mices (Figure 11A). Meanwhile, compound **12u** could also reduce serum total cholesterol concentration with the reduction from 12.7 to 17.2%, respectively (Figure 11B). However, GS decreased the levels of serum triglycerides (53.7%, Figure 11A) and increased serum total cholesterol (6.4%, Figure 11B) at a dose of 100 mg/kg, and this result was in agreement with that reported in recent literature.[34] We also determined hepatic TG and TC in compound **12u**-treated mices. Compared with vehicle mices, compound **12u** largely reduce the contents of triglyceride and total cholesterol (43.5 to 69.7% and 33.5 to 47.5%, respectively) dose-dependently at doses of 50 and 100 mg/kg, respectively (Figure 11C,D). However, GS decreased the contents of triglyceride (45.1%) and total cholesterol (26.3%) (Figures 11C,D) at the dose of 100 mg/kg. On the basis of the above results, we concluded that compound **12u** had more beneficial effects on lowering the contents of serum and hepatic triglycerides and total cholesterol than the naturally occurring

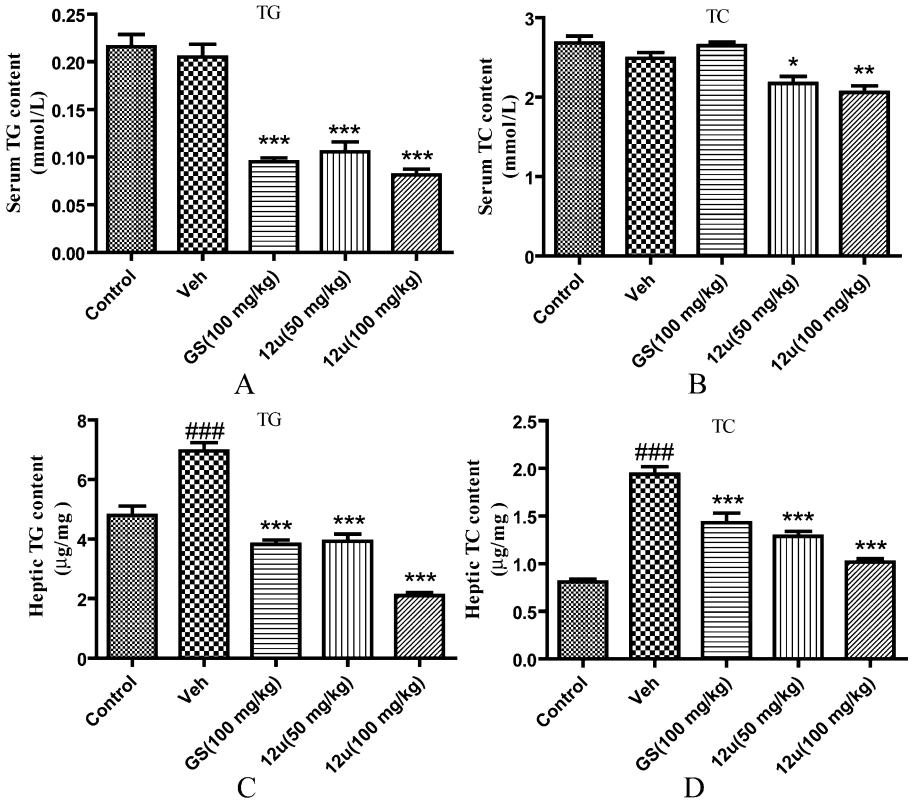

Figure 11. Compound **12u** effectively lowers serum and hepatic triglyceride (A, C) and total cholesterol (B, D) dose-dependently in the cholesterol-fed C57BL/6 mices. Animals were randomly divided into five groups. Animals in the control group were fed a ground-chow diet, and the other four groups were fed a ground-chow diet containing 2% content of cholesterol. GS (100 mg/kg) and compound **12u** (50 and 100 mg/kg) were resuspended in 0.5% CMC-Na and administered to animals by oral gavage. Control animals and vehicle animals were all received the same amount of 0.5% CMC-Na. ###$P < 0.001$ vs control; *$P < 0.05$, **$P < 0.01$ and ***$P < 0.001$ vs vehicle.

FXR antagonist GS. Because of its potency and attractive selectivity profiles, compound **12u** was evaluated in the in vivo rat PK model. Unfortunately, compound **12u** was low aqueous solubility and suffered from poor PK profiles with <5% oral bioavailability in rat (Supporting Information, Tables 4S−5S). We will concentrate our efforts to investigate alternative derivative scaffolds for better PK profiles in future work.

3.4. SAR. The SAR analysis of a set of 27 compounds provided important insights of the essential structural requirements for effective FXR antagonists. An analysis of the data shown in Table 1 reveals some noteworthy observations of the SAR for compounds **11** and **12a−z**: (1) when only R_4 was changed, replacement of the 3′-carbonyl substituent on the phenyl ring with other substituents substantially decreased the antagonistic activities of derivatives (**1** vs **12b** or **12h** or **12j−s**); (2) when only R_1 was changed, 4′-*O*-substitutions on the phenyl ring substantially impacted the antagonistic activities of derivatives, generally, bulky substituents (**12f−g** vs **11** or **12c−e**) are beneficial, (3) introduction of a more double-bond between R_1 and pyrazolone can be tolerated (**11** vs **12i**), (4) aryl substituents at 3-position (R_3) of the pyrazolone framework substantially increased potency (**12u** vs **11** or **12v**), while, in this case, R_4-substitution (**12u**) was not 3′-carbonyl substituted phenyl ring (see the above (1)) and R_1-substitution (**12u**) does not contain 4′-*O*-bulky substitutions on the phenyl ring (see the above (2)). Taken together, the SAR are mixed. A subtle interplay between steric/hydrophobic effects of R_1/R_3 substituent and polarity/hydrogen-bonding capability of R_4 substituent seemed to be critical for high potency. Compounds **12u** represented seemingly the best combination, leading to ∼8-fold potency improvement compared to the lead compound **11**.

3.5. Binding Models. To understand the structural basis for the above SAR, we scrutinized the binding poses of hit compound **11** and the most potent derivative **12u** by means of molecular docking. The top ranking poses of compounds **11** and **12u** were predicted by the docking model generated from chain A of 3DCT[35] and 3RUU,[36] respectively. Figure 12 shows the predicted binding poses of **11** (Figure 12A,B) and **12u** (Figure 12C,D) in FXR ligand binding site. For the compound **11**, 3′-carbonyl substituent on the phenyl ring (region A, Figure 3) forms two strong hydrogen bonds with Arg331 of helix 5 (Figure 12A,B), which is observed for several FXR ligands such as GW4064. Other atoms of compound **11** contribute to interactions only by shape complementary and hydrophobic interaction. A large spatial volume within FXR active site around the ethoxyl group of compound **11** (R_1 in Table1) was available to accommodate large chemical moieties (Figure 12A). The molecular binding model of **11** was in good agreement with the above SARs (1−3). It is notable that compound **11** had no interaction with the AF2 helix, which is considered essential to FXR activation. This might be a reason that compound **11** acts as an FXR antagonist. For compound **12u**, The R_3 of **12u** (phenyl, Table 1) was too large to be accommodated in the binding site of FXR around the methyl group of compound **11** (Figure 12A), hence the pyrazolone framework shifts to the left and takes a different orientation compared to compound **11**, and the nitro group of **12u** is

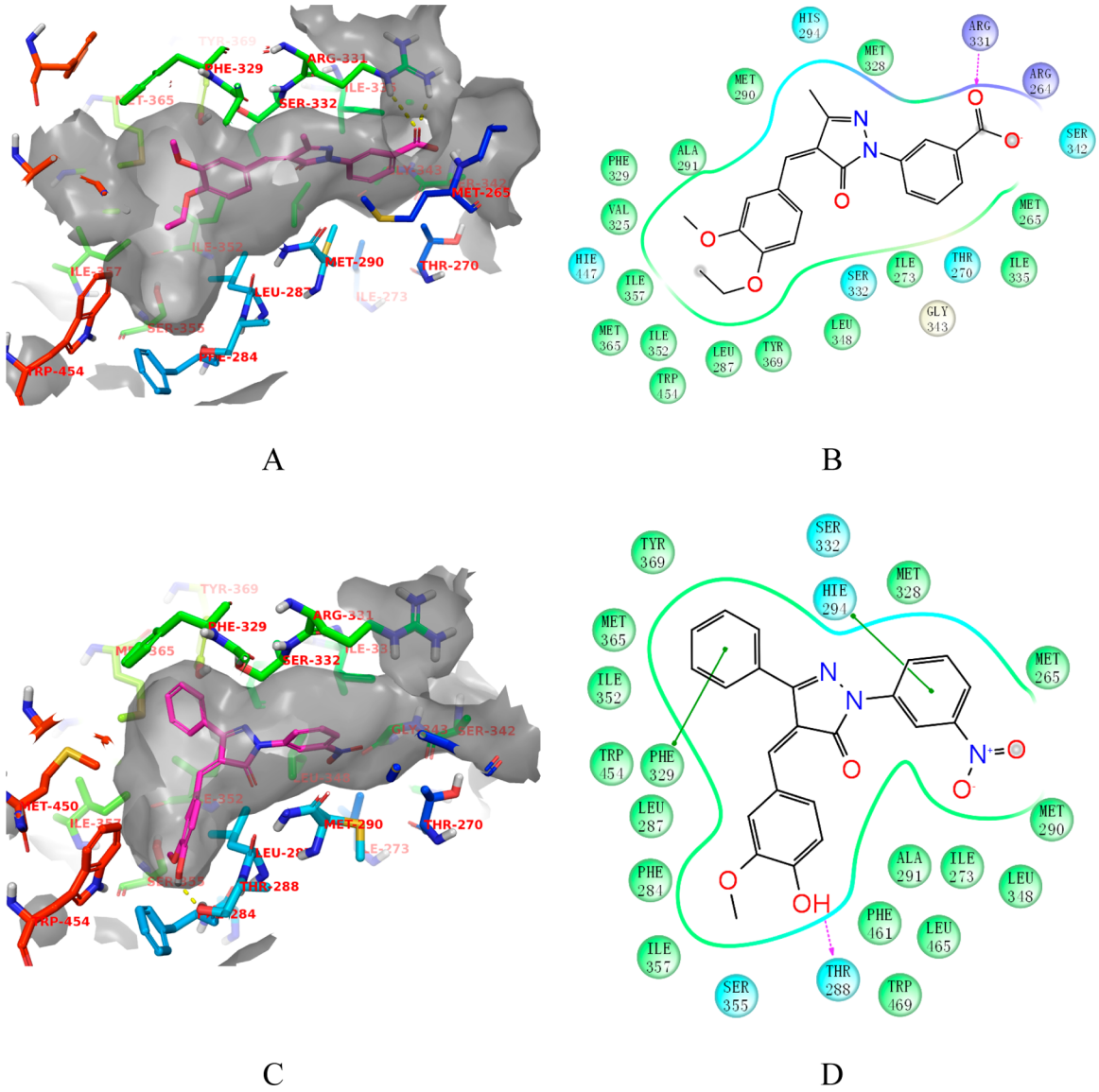

Figure 12. Two-dimensional (2D) and three-dimensional (3D) interaction schemes of predicted binding poses of **11** (A–B) and **12u** (C–D) in FXR active site. The figures were prepared using PyMol (A,C) and Schrodinger Maestro (B,D). In the 2D diagram, magentas dash line with arrow denotes hydrogen bond between ligand and side chain atoms of protein residue, while the green line with arrow denotes the T-shaped π–π interaction from the ligand to the side chain aromatic ring of protein residue. Hydrogen bonds are shown as dotted lines in the 3D views. Critical residues of the binding pocket are labeled in 2D and 3D views.

devoid of hydrogen bond interactions with Arg331 of helix 5 (Figure 12C,D). In recompense for this hydrogen bond loss, the 4′-hydroxy of arylidene moiety (region C, Figure 3) formed one new hydrogen bond with side chain hydroxy of Thr288. In addition, two pairs of T-shaped π–π interactions exist between two phenyl rings of **12u** (R_3 and R_4, Table 1) and two aromatic residues (Phe329 and His294, respectively) (Figure 12D), the additional interaction was regarded as one of the key factors leading to ∼8-fold potency improvement of **12u** compared to **11**. The binding model of **12u** powerfully supports the above SAR (4). It is also worth noting that some AF2 helix residues (Phe461, Leu465, and Trp469) are involved in the hydrophobic interaction with **12u** (Figure 12D). On the basis of the fact that both **11** and **12u** are FXR antagonists, and the observation that known FXR agonists (including CDCA) typically have interaction to both helix 5 (hydrogen bond) and AF2 helix (hydrophobic interaction), it may be hypothesized that the lack of synergetic interactions to both helix 5 and AF2 helix results in antagonistic effect of FXR ligand.

4. CONCLUSION

In summary, we have discovered a new kind of nonsteroidal, selective FXR antagonists by using LBVS approach in conjunction with chemical synthesis and bioassay. On the basis of the structure of lead compound **11**, totally, 26 new derivatives have been synthesized and tested with HTRF-based FXR coactivator association assay. Finally, five derivatives (**12f–g**, **12p**, **12u**, and **12y**) were found to show better antagonistic activities against FXR than compound **11**. Remarkably, the most potent derivative **12u** showed antagonistic capability approximately 10 times and 8 times higher than that of the control GS and prototype compound **11**, respectively. The preliminary SARs were obtained, which show changes of substituents on the 1 (R_4), 3 (R_3), and 4 (R_1)

-positions of pyrazolone moiety, have very important influence on antagonistic activity, and appropriate structural optimizations on the above regions can substantially improve potency.

In several molecular and cellular assays, the derivative **12u** (60 μM) was further confirmed to have high binding affinity with FXRαLBD and could result in 100% inhibition of FXR transactivation induced by 20 μM CDCA. Interestingly, the antagonistic activity of compound **12u** was also observed for FXR specificity over a number of nuclear receptors including RXRα, LXRα, GR, PR, and PPARδ, which was in good agreement with the antagonistic activity of compound **12u** against FXR by strongly reversing the regulating effects of CDCA on FXR target genes (Cyp7A1, SHP, BSEP, and SREBP1c). Further, the therapeutic potential of compound **12u** (10 μM) was identified by lowering the contents of triglyceride and total cholesterol in human hepatoma HepG2 cells, with a similar potency to that of 40 μM GS. The pharmacological results in vivo also showed that compound **12u** had more beneficial effects on lowering the contents of serum and hepatic triglycerides and total cholesterol than FXR natural antagonist GS. Altogether, these data demonstrate that compound **12u** may be a good lead for discovering potential therapeutic drugs for hypercholesterolemia. Considering only a few nonsteroidal, selective FXR antagonists reported so far, compound **12u** can be an effective chemical biology tool for the study of FXR mechanism in the diseases. Further structural optimization of the representative compound **12u** is in progress in our laboratory.

5. EXPERIMENTAL SECTION

5.1. General. The reagents (chemicals) were purchased from Lancaster, Alfa Aesar, Acros, and Shanghai Chemical Reagent Co. and used without further purification. Analytical thin-layer chromatography (TLC) was HSGF 254 (150−200 μm thickness; Yantai Huiyou Co., China). Yields were not optimized. Melting points were measured in capillary tube on a SGW X-4 melting point apparatus without correction. Nuclear magnetic resonance (NMR) spectroscopy was performed on a Bruker AMX-400 NMR (IS as TMS). Chemical shifts were reported in parts per million (ppm, δ) downfield from tetramethylsilane. Proton coupling patterns were described as singlet (s), doublet (d), triplet (t), quartet (q), multiplet (m), and broad (br). Low- and high-resolution mass spectra (LRMS and HRMS) were given with electric ionization (EI) produced by a Finnigan MAT-95. Microwave experiments were carried out in a domestic microwave oven (Midea MM721AAU-PW). Compounds **11** and **12a−z** were confirmed 95% purity (Supporting Information, Table 3S). The details for purity analyses of compounds **11** and **12a−z** are described in the Supporting Information.

*5.1.1. (Z)-3-(4-(4-Ethoxy-3-methoxybenzylidene)-3-methyl-5-oxo-4,5-dihydro-1H-pyrazol-1-yl)benzoic Acid (**11**).* A one-neck 50 mL flask containing 3-methoxy-4-ethoxy-benzaldehyde (**13a**, 54 mg, 0.3 mmol), ethyl acetoacetate (**14a**, 58.5 mg, 0.45 mmol), and 3-hydrazinylbenzoic acid (**15a**, 45.6 mg, 0.3 mmol) was placed in a domestic microwave oven and irradiated at a power of 420 W for 10 min. The solid obtained after cooling was triturated with ethyl acetate and collected by suction filtration to afford product **11** (112 mg, yield 98%) as an orange solid; mp 276−278 °C. ^{1}H NMR (400 MHz, DMSO): δ 1.38 (t, 3H), 2.34 (s, 3H), 3.88 (s, 3H), 4.17 (q, 2H), 7.16 (d, 1H), 7.56 (t, 1H), 7.77 (s, 2H), 8.12 (d, 1H), 8.21 (d, 1H), 8.51 (s, 1H), 8.75 (s, 1H), 13.05 (s, 1H). EI-MS m/z 380 (M$^+$, 100%). HRMS (EI) m/z calcd $C_{21}H_{20}N_2O_5$ (M$^+$) 380.1372, found 380.1371.

*5.1.2. (Z)-4-Benzylidene-3-methyl-1-phenyl-1H-pyrazolidinyl-5(4H)-ketone (**12a**).* **12a** was obtained in the same manner described in the preparation of **11** from ethyl acetoacetate, phenylhydrazine, and benzaldehyde. Yield 47%; mp 103−107 °C. ^{1}H NMR (400 MHz, $CDCl_3$): δ 2.38 (s, 3H), 7.20 (t, 1H), 7.41−7.54 (m, 6H), 7.97 (d, 2H), 8.51 (d, 2H). EI-MS m/z 262 (M$^+$, 100%). HRMS (EI) m/z calcd $C_{17}H_{14}N_2O$ (M$^+$) 262.1106, found 262.1107.

*5.1.3. (Z)-4-(4-Ethoxy-3-methoxybenzylidene)-3-methyl-1-phenyl-1H-pyrazol-5(4H)-one (**12b**).* **12b** was obtained in the same manner described in the preparation of **11** from ethyl acetoacetate, phenylhydrazine, and 3-methoxy-4-ethoxy-benzaldehyde. Yield 63%; mp 134−139 °C. ^{1}H NMR (400 MHz, $CDCl_3$): δ 1.54 (t, 3H), 2.36 (s, 3H), 4.05 (s, 3H), 4.23 (q, 2H), 6.95 (d, 1H), 7.19 (t, 1H), 7.32 (s, 1H), 7.42 (t, 2H), 7.72 (d, 1H), 7.97 (d, 2H), 8.98 (s, 1H). EI-MS m/z 336 (M$^+$, 100%). HRMS (EI) m/z calcd $C_{20}H_{20}N_2O_3$ (M$^+$) 336.1474, found 336.1475.

*5.1.4. (Z)-3-(4-(4-Hydroxy-3-methoxybenzylidene)-3-methyl-5-oxo-4,5-dihydro-1H-pyrazol-1-yl)benzoic Acid (**12c**).* **12c** was obtained in the same manner described in the preparation of **11** from ethyl acetoacetate, 3-hydrazinylbenzoic acid, and 4-hydroxy- 3-methoxybenzaldehyde. Yield 68%; mp 255−257 °C. ^{1}H NMR (400 MHz, DMSO): δ 2.33 (s, 3H), 3.90 (s, 3H), 6.96 (d, 1H), 7.56 (t, 1H), 7.70 (s, 1H), 7.75 (d, 1H), 8.04 (d, 1H), 8.21 (d, 1H), 8.53 (s, 1H), 8.76 (s, 1H). EI-MS m/z 352 (M$^+$, 100%). HRMS (EI) m/z calcd $C_{19}H_{16}N_2O_5$ (M$^+$) 352.1059, found 352.1057.

*5.1.5. (Z)-3-(4-(3,4-Dihydroxybenzylidene)-3-methyl-5-oxo-4,5-dihydro-1H-pyrazol-1-yl)benzoic Acid (**12d**).* **12d** was obtained in the same manner described in the preparation of **11** from ethyl acetoacetate, 3-hydrazinylbenzoic acid, and 3,4-dihydroxy benzaldehyde. Yield 73%; mp 278−280 °C. ^{1}H NMR (400 MHz, DMSO): δ 2.34 (s, 3H), 6.93 (d, 1H), 7.57 (t, 1H), 7.65 (s, 1H), 7.76 (d, 1H), 7.92 (d, 1H), 8.18 (d, 1H), 8.52 (s, 1H), 8.63 (s, 1H), 10.45(s,1H). EI-MS m/z 338 (M$^+$, 100%). HRMS (EI) m/z calcd $C_{18}H_{14}N_2O_5$ (M$^+$) 338.0903, found 338.0782.

*5.1.6. (Z)-3-(4-(4-Isopropoxy-3-methoxybenzylidene)-3-methyl-5-oxo-4,5-dihydro-1H-pyrazol-1-yl)benzoic Acid (**12e**).* **12e** was obtained in the same manner described in the preparation of **11** from ethyl acetoacetate, 3-hydrazinylbenzoic acid, and 4-iso propoxy-3-methoxybenzaldehyde. Yield 76%; mp 206−208 °C. ^{1}H NMR (400 MHz, DMSO): δ 1.33 (s, 6H), 2.36 (s, 3H), 3.87 (s, 3H), 4.83 (m, 1H), 7,21 (d, 1H), 7.57 (t,1H), 7.76 (d, 1H), 7.79 (s, 1H), 8.15 (d, 1H), 8.22 (d, 1H), 8.53 (s, 1H), 8.75 (s, 1H). EI-MS m/z 394 (M$^+$, 100%). HRMS (EI) m/z calcd $C_{22}H_{22}N_2O_5$ (M$^+$) 394.1529, found 394.1528.

*5.1.7. (Z)-3-(4-(3-Methoxy-4-(pentyloxy)benzylidene)-3-methyl-5-oxo-4,5-dihydro-1H-pyrazol-1-yl)benzoic Acid (**12f**).* **12f** was obtained in the same manner described in the preparation of **11** from ethyl acetoacetate, 3-hydrazinylbenzoic acid, and 3-methoxy- 4-(pentyloxy)benzaldehyde. Yield 83%; mp 224−226 °C. ^{1}H NMR (400 MHz, DMSO): δ 0.91 (t, 3H), 1.32−1.43 (m, 4H), 1.77 (m, 2H), 2.35 (s, 3H), 3.88 (s, 3H), 4.11 (t, 2H), 7.18 (d,1H), 7.57 (t, 1H), 7.77 (d, 2H), 8.13 (d, 1H), 8.22 (d, 1H), 8.52 (s, 1H), 8.77 (s, 1H). EI-MS m/z 422 (M$^+$, 100%). HRMS (EI) m/z calcd $C_{24}H_{26}N_2O_5$ (M$^+$) 422.1842, found 422.1840.

*5.1.8. (Z)-3-(4-(4-(Benzyloxy)-3-methoxybenzylidene)-3-methyl-5-oxo-4,5-dihydro-1H-pyrazol-1-yl)benzoic Acid (**12g**).* **12g** was obtained in the same manner described in the preparation of **11** from ethyl acetoacetate, 3-hydrazinylbenzoic acid, and 4-(benzyloxy)-3-methoxybenzaldehyde. Yield 84%; mp 249−252 °C. ^{1}H NMR (400 MHz, DMSO): δ 2.35 (s, 3H), 3.89 (s, 3H), 5.26 (s, 2H), 7.28−7.50 (m, 7H), 7.57 (t, 1H), 7.77 (d, 2H), 8.14 (d, 1H), 8.22 (d, 1H), 8.52 (s, 1H), 8.77 (s, 1H). EI-MS m/z 442 (M$^+$, 100%). HRMS (EI) m/z calcd $C_{26}H_{22}N_2O_5$ (M$^+$) 442.1529, found 442.1530.

*5.1.9. (Z)-4-(4-Ethoxy-3-methoxybenzylidene)-3-methyl-1-(3-nitrophenyl)- pyrazol-5(4H)-one (**12j**).* **12j** was obtained in the same manner described in the preparation of **11** from ethyl acetoacetate, (3-nitrophenyl)hydrazine, and 3-methoxy-4-ethoxy-benzaldehyde. Yield 83%; mp 212−213 °C. ^{1}H NMR (400 MHz, $CDCl_3$): δ 1.55 (t, 3H), 2.38 (s, 3H), 4.07 (s, 3H), 4.27 (q, 2H), 6.98 (d, 1H), 7.37 (s, 1H), 7.59 (t, 1H), 7.75 (d, 1H), 8.03 (d, 1H), 8.47 (d, 1H), 8.93 (d, 2H). EI-MS m/z 381 (M$^+$, 100%). HRMS (EI) m/z calcd $C_{20}H_{19}N_3O_5$ (M$^+$) 381.1325, found 381.1321.

*5.1.10. (Z)-4-(4-Ethoxy-3-methoxybenzylidene)-3-methyl-1-(4-nitrophenyl)-1H-pyrazol-5(4H)-one (**12k**).* **12k** was obtained in the same manner described in the preparation of **11** from ethyl acetoacetate, (4-nitrophenyl)hydrazine, and 3-methoxy-4-ethoxy-ben-

zaldehyde. Yield 78%; mp 213−215 °C. ^{1}H NMR (400 MHz, $CDCl_3$): δ 1.55 (t, 3H), 2.38 (s, 3H), 4.06 (s, 3H), 4.25 (q, 2H), 6.97 (d, 1H), 7.37 (s, 1H), 7.73 (d, 1H), 8.29 (s, 4H), 8.90 (s, 1H). EI-MS *m/z* 381 (M^+, 100%). HRMS (EI) *m/z* calcd $C_{20}H_{19}N_3O_5$ (M^+) 381.1325, found 381.1323.

*5.1.11. (Z)-4-(4-Ethoxy-3-methoxybenzylidene)-3-methyl-1-(3-(trifluoromethyl)phenyl)-1H-pyrazol-5(4H)-one (**12l**).* **12l** was obtained in the same manner described in the preparation of **11** from ethyl acetoacetate, (3-(trifluoromethyl)phenyl)hydrazine, and 3-methoxy-4-ethoxy-benzaldehyde. Yield 67%; mp 147−151 °C. ^{1}H NMR (400 MHz, $CDCl_3$): δ 1.54 (t, 3H), 2.37 (s, 3H), 4.06 (s, 3H), 4.24 (q, 2H), 6.97 (d, 1H), 7.35 (s, 1H), 7.42 (d, 1H), 7.53 (t, 1H), 7.75 (d, 1H), 8.28 (d, 1H), 8.31 (s, 1H), 8.91 (s, 1H). EI-MS *m/z* 404 (M^+, 100%). HRMS (EI) *m/z* calcd $C_{21}H_{19}F_3N_2O_3$ (M^+) 404.1348, found 404.1349.

*5.1.12. (Z)-4-(4-Ethoxy-3-methoxybenzylidene)-3-methyl-1-(4-(trifluoromethyl)phenyl)-1H-pyrazol-5(4H)-one (**12m**).* **12m** was obtained in the same manner described in the preparation of **11** from ethyl acetoacetate, (4-(trifluoromethyl)phenyl)hydrazine, and 3-methoxy-4-ethoxy-benzaldehyde. Yield 53%; mp 144−147 °C. ^{1}H NMR (400 MHz, $CDCl_3$): δ 1.54 (t, 3H), 2.37 (s, 3H), 4.05 (s, 3H), 4.25 (q, 2H), 6.96 (d, 1H), 7.35 (s, 1H), 7.66 (d, 2H), 7.72 (d, 1H), 8.18 (d, 2H), 8.93 (s, 1H). EI-MS *m/z* 404 (M^+, 100%). HRMS (EI) *m/z* calcd $C_{21}H_{19}F_3N_2O_3$ (M^+) 404.1348, found 404.1349.

*5.1.13. (Z)-1-(3,5-Bis(trifluoromethyl)phenyl)-4-(4-ethoxy-3-methoxybenzylidene)-3-methyl-1H-pyrazol-5(4H)-one (**12n**).* **12n** was obtained in the same manner described in the preparation of **11** from ethyl acetoacetate, (3,5-bis(trifluoromethyl)phenyl) hydrazine, and 3-methoxy-4-ethoxy-benzaldehyde. Yield 54%; mp 198−200 °C. ^{1}H NMR (400 MHz, $CDCl_3$): δ 1.54 (t, 3H), 2.38 (s, 3H), 4.07 (s, 3H), 4.25 (q, 2H), 6.98 (d, 1H), 7.37 (s, 1H), 7.65 (s, 1H), 7.77 (d, 1H), 8.61 (s, 2H), 8.84 (s, 1H). EI-MS *m/z* 472 (M^+, 100%). HRMS (EI) *m/z* calcd $C_{22}H_{18}F_6N_2O_3$ (M^+) 472.1222, found 472.1223.

*5.1.14. (Z)-4-(4-Ethoxy-3-methoxybenzylidene)-1-(2-fluorophenyl)-3-methyl-1H-pyrazol-5(4H)-one (**12o**).* **12o** was obtained in the same manner described in the preparation of **11** from ethyl acetoacetate, (2-fluorophenyl)hydrazine, and 3-methoxy-4-ethoxy-benzaldehyde. Yield 51%; mp 153−155 °C. ^{1}H NMR (400 MHz, $CDCl_3$): δ 1.52 (t, 3H), 2.34 (s, 3H), 4.00 (s, 3H), 4.22 (q, 2H), 6.93 (d, 1H), 7.22 (q, 2H), 7.32 (t, 1H), 7.36 (s, 1H), 7.52 (t, 1H), 7.67 (d, 1H). EI-MS *m/z* 354 (M^+, 100%). HRMS (EI) *m/z* calcd $C_{20}H_{19}FN_2O_3$ (M^+) 354.1380, found 354.1377.

*5.1.15. (Z)-4-(4-Ethoxy-3-methoxybenzylidene)-3-methyl-1-perfluorophenyl-1H-pyrazol-5(4H)-one (**12p**).* **12p** was obtained in the same manner described in the preparation of **11** from ethyl acetoacetate, (perfluorophenyl)hydrazine, and 3-methoxy-4-ethoxy-benzaldehyde. Yield 60%; mp 169−171 °C. ^{1}H NMR (400 MHz, $CDCl_3$): δ 1.53 (t, 3H), 2.35 (s, 3H), 4.00 (s, 3H), 4.23 (q, 2H), 6.95 (d, 1H), 7.41 (s, 1H), 7.63 (d, 1H), 8.96 (s, 1H). EI-MS *m/z* 426 (M^+, 100%). HRMS (EI) *m/z* calcd $C_{20}H_{15}F_5N_2O_3$ (M^+) 426.1003, found 426.1002.

*5.1.16. (Z)-1-(3,4-Dichlorophenyl)-4-(4-ethoxy-3-methoxybenzylidene)-3-methyl-1H-pyrazol-5(4H)-one (**12q**).* **12q** was obtained in the same manner described in the preparation of **11** from ethyl acetoacetate, (3,4-dichlorophenyl)hydrazine, and 3-methoxy-4-ethoxy-benzaldehyde. Yield 86%; mp 164−166 °C. ^{1}H NMR (400 MHz, $CDCl_3$): δ 1.53 (t, 3H), 2.34 (s, 3H), 4.05 (s, 3H), 4.23 (q, 2H), 6.95 (d, 1H), 7.32 (s, 1H), 7.44 (s, 1H), 7.71 (d, 1H), 7.94 (d, 1H), 8.21 (s, 1H), 8.90 (s, 1H). EI-MS *m/z* 404 (M^+, 100%). HRMS (EI) *m/z* calcd $C_{20}H_{18}Cl_2N_2O_3$ (M^+) 404.0694, found 404.0695.

*5.1.17. (Z)-1-(3,5-Dichlorophenyl)-4-(4-ethoxy-3-methoxybenzylidene)-3-methyl-1H-pyrazol-5(4H)-one (**12r**).* **12r** was obtained in the same manner described in the preparation of **11** from ethyl acetoacetate, (3,5-dichlorophenyl)hydrazine, and 3-methoxy-4-ethoxy-benzaldehyde. Yield 73%; mp 182−185 °C. ^{1}H NMR (400 MHz, $CDCl_3$): δ 1.54 (t, 3H), 2.35 (s, 3H), 4.06 (s, 3H), 4.23 (q, 2H), 6.96 (d, 1H), 7.15 (s, 1H), 7.33 (s, 1H), 7.72 (d, 1H), 8.04 (s, 2H), 8.89 (s, 1H). EI-MS *m/z* 404 (M^+, 100%). HRMS (EI) *m/z* calcd $C_{20}H_{18}Cl_2N_2O_3$ (M^+) 404.0694, found 404.0697.

*5.1.18. (Z)-4-(4-Ethoxy-3-methoxybenzylidene)-1-(4-isopropylphenyl)-3-methyl-1H-pyrazol-5(4H)-one (**12s**).* **12s** was obtained in the same manner described in the preparation of **11** from ethyl acetoacetate, (4-isopropylphenyl)hydrazine, and 3-methoxy-4-ethoxy-benzaldehyde. Yield 63%; mp 129−131 °C. ^{1}H NMR (400 MHz, $CDCl_3$): δ 1.26 (d, 6H), 1.53 (t, 3H), 2.34 (s, 3H), 2.93 (m, 1H),4.04 (s, 3H), 4.22 (q, 2H), 6.94 (d, 1H), 7.30 (d, 2H), 7.70 (d, 1H), 7.83 (d, 2H), 9.01 (s, 1H). EI-MS *m/z* 378 (M^+, 100%). HRMS (EI) *m/z* calcd $C_{23}H_{26}N_2O_3$ (M^+) 378.1943, found 378.1942.

*5.1.19. (Z)-4-((4-Methoxynaphthalen-1-yl)methylene)-3-methyl-1-(3-nitrophenyl)-1H-pyrazol-5(4H)-one (**12t**).* **12t** was obtained in the same manner described in the preparation of **11** from ethyl acetoacetate, (3-nitrophenyl)hydrazine, and 4-methoxy-1- naphthaldehyde. Yield 70%; mp 236−237 °C. ^{1}H NMR (400 MHz, $CDCl_3$): δ 2.51 (s, 3H), 4.16 (s, 3H), 7.05 (d, 1H), 7.57 (t, 1H), 7.72 (t, 1H), 8.02 (q, 2H), 8.15 (d, 1H), 8.33 (s, 1H), 8.41 (d, 1H), 8.48 (d, 1H), 8.96 (t, 1H), 9.40 (d, 1H). EI-MS *m/z* 387 (M^+, 100%). HRMS (EI) *m/z* calcd $C_{22}H_{17}N_3O_4$ (M^+) 387.1219, found 387.1212.

*5.1.20. (Z)-4-(4-Hydroxy-3-methoxybenzylidene)-1-(3-nitrophenyl)-3-phenyl-1H-pyrazol-5(4H)-one (**12u**).* **12u** was obtained in the same manner described in the preparation of **11** from ethyl 3-oxo-3-phenylpropanoate, (3-nitrophenyl)hydrazine, and 4-hydroxy-3-methoxybenzaldehyde. Yield 61%; mp 199−202 °C. ^{1}H NMR (400 MHz, $CDCl_3$): δ 4.14 (s, 3H), 6.38 (s, 1H), 7.03 (d, 1H), 7.53 (d, 1H), 7.56 (m, 4H), 7.69 (d, 1H), 7.71 (d, 1H), 8.07 (d, 1H), 8.54 (d, 1H), 9.06 (s, 1H), 9.15 (s, 1H). EI-MS *m/z* 415 (M^+, 100%). HRMS (EI) *m/z* calcd $C_{23}H_{17}N_3O_5$ (M^+) 415.1168, found 415.1159.

*5.1.21. (Z)-4-(4-Hydroxy-3-methoxybenzylidene)-3-isopropyl-1-(3-nitrophenyl)-1H-pyrazol-5(4H)-one (**12v**).* **12v** was obtained in the same manner described in the preparation of **11** from ethyl 4-methyl-3-oxopentanoate, (3-nitrophenyl)hydrazine, and 3-methoxy benzaldehyde. Yield 67%; mp 200−201 °C. ^{1}H NMR (400 MHz, $CDCl_3$): δ 1.42 (s, 3H), 1.43 (s, 3H), 3.14 (m, 1H), 4.11 (s, 3H), 6.36 (s, 1H), 7.04 (d, 1H), 7.43 (s, 1H), 7.55 (d, 1H), 7.59 (t, 1H), 8.03 (d, 1H), 8.48 (d, 1H), 8.96 (t, 1H), 9.17 (s, 1H). EI-MS *m/z* 381.1 (M^+, 100%). HRMS (EI) *m/z* calcd $C_{20}H_{19}N_3O_5$ (M^+) 381.1325, found 381.1315.

*5.1.22. (Z)-3-Methyl-4-((5-methylthiophen-2-yl)methylene)-1-(3-nitrophenyl)-1H-pyrazol-5(4H)-one (**12w**).* **12w** was obtained in the same manner described in the preparation of **11** from ethyl acetoacetate, (3-nitrophenyl)hydrazine, and 5-methylthiophene- 2-carbaldehyde. Yield 53%; mp 199−201 °C. ^{1}H NMR (400 MHz, $CDCl_3$): δ 2.39 (s, 1H), 2.67 (s, 3H), 7.00 (s, 1H), 7.58 (t, 2H), 7.85 (s, 1H), 8.02 (d, 1H), 8.53 (d, 1H), 8.92 (s, 1H). EI-MS *m/z* 327 (M^+, 100%). HRMS (EI) *m/z* calcd $C_{16}H_{13}N_3O_3S$ (M^+) 327.0678, found 327.0675.

*5.1.23. (Z)-4-(1-(4-Chlorophenyl)ethyliden-1-yl)-3-methyl-1-(4-nitrophenyl)-1H-pyrazol-5(4H)-one (**12x**).* **12x** was obtained in the same manner described in the preparation of **11** from ethyl acetoacetate, (4-nitrophenyl)hydrazine, and 1-(4-chlorophenyl)-ethanone. Yield 50%; mp 193−196 °C. ^{1}H NMR (400 MHz, DMSO): δ 1.69 (s, 3H), 2.88 (s, 3H), 7.24 (d, 2H), 7.51 (d, 2H), 8.28 (m, 4H). EI-MS *m/z* 355 (M^+, 100%). HRMS (EI) *m/z* calcd $C_{18}H_{14}ClN_3O_3$ (M^+) 355.0742, found 355.0719.

*5.1.24. (Z)-4-(4-Bromobenzylidene)-3-methyl-1-phenyl-1H-pyrazol-5(4H)-one (**12y**).* **12y** was obtained in the same manner described in the preparation of **11** from ethyl acetoacetate, phenylhydrazine, and 4-bromobenzaldehyde. Yield 53%; mp 117−120 °C. ^{1}H NMR (400 MHz, $CDCl_3$): δ 2.36 (s, 3H), 7.21 (t, 1H), 7.32 (s, 1H), 7.43 (t, 2H), 7.65 (d, 2H), 7.95 (d, 2H), 8.39 (d, 2H). EI-MS *m/z* 340 (M^+, 100%). HRMS (EI) *m/z* calcd $C_{17}H_{13}BrN_2O$ (M^+) 340.0211, found 340.0212.

*5.1.25. Ethyl 3-Hydrazinylbenzoate (**16**).* A mixture of 3-hydrazino benzoic acid (0.5 g, 3.3 mmol) and concd H_2SO_4 (0.5 mL) in ethanol (10 mL) was refluxed for 12 h, and most of solvent was evaporated, filtered, washed, and dried to afford **15** (0.38 g, 64%).

*5.1.26. Ethyl 3-(3-Methyl-5-oxo-4,5-dihydro-1H-pyrazol-1-yl)-benzoate (**17**).* A mixture of **16** (0.36 g, 2 mmol) and ethyl acetoacetate (0.26 g, 2 mmol) in acetic acid (10 mL) was heated to reflux for 4 h, poured into H_2O (50 mL), and extracted with EtOAc. The combined organic layer was washed, dried, filtered, and condensed. The residue was purified by flash chromatography on

silica gel, eluted with a mixture of EtOAc/petroleum ether (1:4, v/v), to afford **17** (0.27 g, 77%) as a white solid.

*5.1.27. Ethyl (Z)-3-(4-(4-Ethoxy-3-methoxybenzylidene)-3-methyl-5-oxo-4,5-dihydro-1H-pyrazol-1-yl)benzoate (**12h**).* A mixture of 3-methoxy-4-ethoxy-benzaldehyde (0.18 g, 1 mmol) and **17** (0.25 g, 1 mmol) in ethanol (10 mL) was heated to reflux for 5 h, and most of solvent was evaporated. The residue was purified by flash chromatography on silica gel, eluted with a mixture of EtOAc/petroleum ether (1:10, v/v), to afford **12h** (0.21 g, 52%) as a yellow solid; mp 117−121 °C. ^{1}H NMR (400 MHz, DMSO): δ 1.44 (t, 3H), 1.56 (t, 3H), 2.39 (s, 3H), 4.07 (s, 3H), 4,25 (q, 2H), 4.43 (q, 2H), 6.98 (d, 1H), 7.36 (s, 1H), 7.51 (t, 1H), 7.75 (dd, 1H), 7.89 (d, 1H), 8.26 (d, 1H), 8.62 (t, 1H), 8.99 (d, 1H). EI-MS m/z 408 (M^+, 100%). HRMS (EI) m/z calcd $C_{23}H_{24}N_2O_5$ (M^+) 408.1685, found 408.1682.

*5.1.28. Ethyl (Z)-3-(4-((E)-3-Phenylallylidene)-3-methyl-5-oxo-4,5-dihydro-1H-pyrazol-1-yl)benzoate (**18**).* **18** was obtained in the same manner described in the preparation of **12h** from cinnamaldehyde and **17**; mp 150−152 °C. ^{1}H NMR (400 MHz, $CDCl_3$): δ 1.45 (t, 3H), 2.34 (s, 3H), 4.43 (q, 2H), 7.26 (d, 1H), 7.44−7.52 (m, 4H), 7.70 (dd, 2H), 7.89 (d, 2H), 8.25 (d, 1H), 8.59−8.65 (m, 2H). EI-MS m/z 360 (M^+, 100%). HRMS (EI) m/z calcd $C_{22}H_{20}N_2O_3$ (M^+) 360.1474, found 360.1448.

*5.1.29. (Z)-3-(4-((E)-3-Phenylallylidene)-3-methyl-5-oxo-4,5-dihydro-1H-pyrazol-1-yl)benzoic Acid (**12i**).* A mixture of **18** (180 mg, 0.5 mmol) and LiOH (24 mg, 1 mmol) in THF/methanol/H_2O (3:1:1, v/v/v, 20 mL) was stirred at room temperature for 12 h. The resulting solution was acidified to pH 3 using 1 N HCl. The product was extracted, dried, filtered, concentrated, and purified by flash chromatography using EtOAc/petroleum ether (2:1, v/v), to afford **12i**; mp 232−237 °C. ^{1}H NMR (400 MHz, $CDCl_3$): δ 2.34 (s, 3H), 7.33 (d, 1H), 7.44 (d, 2H), 7.54 (m, 3H), 7.70 (d, 2H), 8.31 (d, 1H), 8.61 (d, 1H), 8.65 (d, 1H), 8.72 (t, 1H). EI-MS m/z 332 (M^+, 100%). HRMS (EI) m/z calcd $C_{20}H_{16}N_2O_3$ (M^+) 332.1161, found 332.1153.

*5.1.30. Isopropyl (Z)-3-(4-(4-Hydroxy-3-methoxybenzylidene)-3-methyl-5-oxo-4,5- dihydro-1H-pyrazol-1-yl)benzoate (**12z**).* **12c** (100 mg, 0.284 mmol) and dried potassium carbonate (59 mg, 0.43 mmol) were dissolved in anhydrous DMF (20 mL), refluxed for 30 min, followed by addition of 2-bromopropane (59 mg, 0.34 mmol), and the reaction was stirred overnight at 60 °C. The reaction mixture was washed with brine and purified by flash chromatography (EtOAc/petroleum ether = 1:4, v/v) on silica gel to afford **12z** (65 mg, 65%) as a yellow solid; mp 129−133 °C. ^{1}H NMR (400 MHz, $CDCl_3$): δ 1.40 (s, 3H), 1.42 (s, 3H), 2.39 (s, 3H), 4.10 (s, 3H), 5.30 (m, 1H), 7.04 (d, 1H), 7.36 (s, 1H), 7.52 (q, 2H), 7.88 (d, 1H), 8.23 (d, 1H), 8.60 (s, 1H), 9.24 (s, 1H). EI-MS m/z 394 (M^+, 100%). HRMS (EI) m/z calcd $C_{22}H_{22}N_2O_5$ (M^+) 394.1529, found 394.1523.

■ ASSOCIATED CONTENT

Supporting Information

Known FXR modulators used in LBVS, distribution of similarity score from LBVS, binding prediction of compounds **11** and **12u**, shape comparison of compound **11** and the matched query antagonist, HPLC reports for the purity check of the compounds **11** and **12a−z**, and pharmacokinetic measurements of compound **12u** in rat. This material is available free of charge via the Internet at http://pubs.acs.org.

■ AUTHOR INFORMATION

Corresponding Author

*For L.C.: phone, +86-21-50806918; E-mail, lilichen@mail.shcnc.ac.cn; address, State Key Laboratory of Drug Research Shanghai Institute of Materia Medica, Chinese Academy of Sciences, 555 Zu Chong Zhi Road, Shanghai 201203, China. For J.L.: phone, +86-21-64252584; fax, +86-21-64252584; E-mail, jianli@ecust.edu.cn; address, Department of Pharmaceutical Sciences School of Pharmacy, East China University of Science and Technology, 130 Mei Long Road, Shanghai 200237, China.

Author Contributions

‖These authors contributed equally to this work.

Notes

The authors declare no competing financial interest.

■ ACKNOWLEDGMENTS

We gratefully acknowledge the financial supports from the National Natural Science Foundation of China (grants 20902022, 81173105, 30890044), National S&T Major Project, China (grants 2011ZX09102-005-02, 2009ZX09103-646), the Shanghai Committee of Science and Technology (grant 11DZ2260600), the 111 Project (grant B07023), Foundation of Chinese Academy of Sciences (grant KSCX2-EW-Q-3), and the Fundamental Research Funds for the Central Universities.

■ ABBREVIATIONS USED

FXR, farnesoid-X-receptor; NR1H4, nuclear receptor subfamily 1 group H member 4; NRs, nuclear receptors; BAs, bile acids; Cyp7A1, liver-specific cholesterol 7α-hydroxylase; NTCP, Na^+-dependent taurocholate cotransporting polypeptide; BSEP, bile salt export pump; HDL, high-density lipoprotein; LDL, low-density lipoprotein; LXR, liver-X-receptor; GS, *Z*-guggulsterone; HTRF, homogeneous time-resolved fluorescence assay; LBVS, ligand-based virtual screening; PDB, Protein Data Bank; LB, Luria−Bertani; GST, glutathione *S*-transferase; CDCA, chenodeoxycholic acid; DSC, differential scanning calorimetry; RXR, retinoid-X-receptor; FXRE, FXR response element; RT-PCR, real-time polymerase chain reaction; BCA, bicinchoninic acid; ACC, acetyl-CoA carboxylase; AceCS, acetyl-CoA synthetase; FAS, fatty acid synthase; SHP, small heterodimer partner; SREBP1c, sterol regulatory element-binding protein 1c; LRMS, low-resolution mass spectra; EI, electric ionization

■ REFERENCES

(1) Parks, D. J.; Blanchard, S. G.; Bledsoe, R. K.; Chandra, G.; Consler, T. G.; Kliewer, S. A.; Stimmel, J. B.; Willson, T. M.; Zavacki, A. M.; Moore, D. D.; Lehmann, J. M. Bile acids: natural ligands for an orphan nuclear receptor. *Science* **1999**, *284*, 1365−1368.

(2) Makishima, M.; Okamoto, A. Y.; Repa, J. J.; Tu, H.; Learned, R. M.; Luk, A.; Hull, M. V.; Lustig, K. D.; Mangelsdorf, D. J.; Shan, B. Identification of a nuclear receptor for bile acids. *Science* **1999**, *284*, 1362−1365.

(3) Cariou, B.; Staels, B. FXR: a promising target for the metabolic syndrome? *Trends Pharmacol. Sci.* **2007**, *28*, 236−243.

(4) Chiang, J. Y.; Kimmel, R.; Weinberger, C.; Stroup, D. Farnesoid X receptor responds to bile acids and represses cholesterol 7alpha-hydroxylase gene (CYP7A1) transcription. *J. Biol. Chem.* **2000**, *275*, 10918−10924.

(5) Myant, N. B.; Mitropoulos, K. A. Cholesterol 7a-hydroxylase. *J. Lipid Res.* **1977**, *18*, 135−153.

(6) Denson, L. A.; Sturm, E.; Echevarria, W.; Zimmerman, T. L.; Makishima, M.; Mangelsdorf, D. J.; Karpen, S. J. The orphan nuclear receptor, shp, mediates bile acid-induced inhibition of the rat bile acid transporter, ntcp. *Gastroenterology* **2001**, *121*, 140−147.

(7) Ananthanarayanan, M.; Balasubramanian, N.; Makishima, M.; Mangelsdorf, D. J.; Suchy, F. J. Human bile salt export pump promoter is transactivated by the farnesoid X receptor/bile acid receptor. *J. Biol. Chem.* **2001**, *276*, 28857−28865.

(8) Wang, Y. D.; Chen, W. D.; Moore, D. D.; Huang, W. FXR: a metabolic regulator and cell protector. FXR: a metabolic regulator and cell protector. *Cell Res.* **2008**, *18*, 1087−1095.

(9) Fiorucci, S.; Mencarelli, A.; Palladino, G.; Cipriani, S. Bile-acid activated receptors: targeting TGR5 and farnesoid-X-receptor in lipid and glucose disorders. *Trends Pharmacol. Sci.* **2009**, *30*, 570−580.

(10) Bishop-Bailey, D.; Walsh, D. T.; Warner, T. D. Expression and activation of the farnesoid X receptor in the vasculature. *Proc. Natl. Acad. Sci. U.S.A.* **2004**, *101*, 3668−3673.
(11) Huang, W.; Ma, K.; Zhang, J.; Qatanani, M.; Cuvillier, J.; Liu, J.; Dong, B.; Huang, X.; Moore, D. D. Nuclear receptor-dependent bile acid signaling is required for normal liver regeneration. *Science* **2006**, *312*, 233−236.
(12) Yang, F.; Huang, X.; Yi, T.; Yen, Y.; Moore, D. D.; Huang, W. Spontaneous development of liver tumors in the absence of the bile acid receptor farnesoid X receptor. *Cancer Res.* **2007**, *67*, 863−867.
(13) Modica, S.; Murzilli, S.; Salvatore, L.; Schmidt, D. R.; Moschetta, A. Nuclear bile acid receptor FXR protects against intestinal tumorigenesis. *Cancer Res.* **2008**, *68*, 9589−9594.
(14) Fiorucci, S.; Mencarelli, A.; Distrutti, E.; Palladino, G.; Cipriani, S. Targeting farnesoid-X-receptor: from medicinal chemistry to disease treatment. *Curr. Med. Chem.* **2010**, *17*, 139−159.
(15) Fiorucci, S.; Cipriani, S.; Baldelli, F.; Mencarelli, A. Bile acid activated receptors in the treatment of dyslipidemia and related disorders. *Prog. Lipid Res.* **2010**, *49*, 171−185.
(16) Fiorucci, S.; Baldelli, F. Farnesoid X receptor agonists in biliary tract disease. *Curr. Opin. Gastroenterol.* **2009**, *25*, 252−259.
(17) Fiorucci, S.; Rizzo, G.; Donini, A.; Distrutti, E.; Santucci, L. Targeting farnesoid X receptor for liver and metabolic disorders. *Trends Mol. Med.* **2007**, *13*, 298−309.
(18) Fiorucci, S.; Cipriani, S.; Mencarelli, A.; Baldelli, F.; Bifulco, G.; Zampella, A. Farnesoid X Receptor Agonist for the Treatment of Liver and Metabolic Disorders: Focus on 6-Ethyl-CDCA. *Mini-Rev. Med. Chem.* **2011**, *11*, 753−762.
(19) Urizar, N. L.; Liverman, A. B.; Dodds, D. T.; Silva, F. V.; Ordentlich, P.; Yan, Y.; Gonzalez, F. J.; Heyman, R. A.; Mangelsdorf, D. J.; Moore, D. D. A natural product that lowers cholesterol as an antagonist ligand for FXR. *Science* **2002**, *296*, 1703−1706.
(20) Verma, A. K.; Khemaria, P.; Gupta, J.; Singh, D. P.; Joshi, B. S.; Roy, R.; Mishra, A. K.; Pratap, R. Bio-transformation of FXR antagonist CDRI 80/574. *ARKIVOC* **2010**, *9*, 1−11.
(21) Sepe, V.; Bifulco, G.; Renga, B.; D'Amore, C.; Fiorucci, S.; Zampella, A. Discovery of sulfated sterols from marine invertebrates as a new class of marine natural antagonists of farnesoid-X-receptor. *J. Med. Chem.* **2011**, *54*, 1314−1320.
(22) Yu, J.; Lo, J. L.; Huang, L.; Zhao, A.; Metzger, E.; Adams, A.; Meinke, P. T.; Wright, S. D.; Cui, J. Lithocholic acid decreases expression of bile salt export pump through farnesoid X receptor antagonist activity. *J. Biol. Chem.* **2002**, *277*, 31441−31447.
(23) Nam, S. J.; Ko, H.; Shin, M.; Ham, J.; Chin, J.; Kim, Y.; Kim, H.; Shin, K.; Choi, H.; Kang, H. Farnesoid X-activated receptor antagonists from a marine sponge *Spongia* sp. *Bioorg. Med. Chem. Lett.* **2006**, *16*, 5398−5402.
(24) Carter, B. A.; Taylor, O. A.; Prendergast, D. R.; Zimmerman, T. L.; Von Furstenberg, R.; Moore, D. D.; Karpen, S. J. Stigmasterol, a soy lipid-derived phytosterol, is an antagonist of the bile acid nuclear receptor FXR. *Pediatr. Res.* **2007**, *62*, 301−306.
(25) Dussault, I.; Beard, R.; Lin, M.; Hollister, K.; Chen, J.; Xiao, J. H.; Chandraratna, R.; Forman, B. M. Identification of gene-selective modulators of the bile acid receptor FXR. *J. Biol. Chem.* **2003**, *278*, 7027−7033.
(26) Kaimal, R.; Song, X.; Yan, B.; King, R.; Deng, R. Differential modulation of farnesoid X receptor signaling pathway by the thiazolidinediones. *J. Pharmacol. Exp. Ther.* **2009**, *330*, 125−134.
(27) Kainuma, M.; Makishima, M.; Hashimoto, Y.; Miyachi, H. Design, synthesis, and evaluation of non-steroidal farnesoid X receptor (FXR) antagonist. *Bioorg. Med. Chem.* **2007**, *15*, 2587−2600.
(28) Sastry, G. M.; Dixon, S. L.; Sherman, W. Rapid shape-based ligand alignment and virtual screening method based on atom/feature-pair similarities and volume overlap scoring. *J. Chem. Inf. Model.* **2011**, *51*, 2455−66.
(29) Ma, R.; Zhu, J.; Liu, J.; Chen, L.; Shen, X.; Jiang., H.; Li, J. Microwave-assisted one-pot synthesis of pyrazolone derivatives under solvent-free conditions. *Molecules* **2010**, *15*, 3593−3601.
(30) Shen, X.; Tomoo, K.; Uchiyama, S.; Kobayashi, Y.; Ishida, T. Structural and thermodynamic behavior of eukaryotic initiation factor 4E in supramolecular formation with 4E-binding protein 1 and mRNA cap analogue, studied by spectroscopic methods. *Chem. Pharm. Bull.* **2001**, *49*, 1299−1303.
(31) Zhang, H.; Zhou, R.; Li, L.; Chen, J.; Chen, L.; Li, C.; Ding, H.; Yu, L.; Hu, L.; Jiang, H.; Shen, X. Danthron functions as an RXR antagonist by stabilizing the receptor's tetramers. *J. Biol. Chem.* **2010**, *286*, 1868−1875.
(32) Renga, B.; Mencarelli, A.; D'Amore, C.; Cipriani, S.; D'Auria, M. V.; Sepe, V.; Chini, M. G.; Monti, M. C.; Bifulco, G.; Zampella, A.; Fiorucci, S. Discovery that theonellasterol a marine sponge sterol is a highly selective FXR antagonist that protects against liver injury in cholestasis. *PLoS One* **2012**, *7*, e30443.
(33) Pellicciari, R.; Costantino, G.; Fiorucci, S. Farnesoid X Receptor: From Structure to Potential Clinical Applications. *J. Med. Chem.* **2005**, *48*, 5383−5403.
(34) Szapary, P. O.; Wolfe, M. L.; Bloedon, L. T.; Cucchiara, A. J.; DerMarderosian, A. H.; Cirigliano, M. D.; Rader, D. J. Guggulipid for the treatment of hypercholesterolemia: a randomized controlled trial. *JAMA, J. Am. Med. Assoc.* **2003**, *290*, 765−772.
(35) Akwabi-Ameyaw, A.; Bass, J. Y.; Caldwell, R. D.; Caravella, J. A.; Chen, L.; Creech, K. L.; Deaton, D. N.; Jones, S. A.; Kaldor, I.; Liu, Y.; Madauss, K. P.; Marr, H. B.; McFadyen, R. B.; Miller, A. B.; Iii, F. N.; Parks, D. J.; Spearing, P. K.; Todd, D.; Williams, S. P.; Wisely, G. B. Conformationally constrained farnesoid X receptor (FXR) agonists: naphthoic acid-based analogs of GW 4064. *Bioorg. Med. Chem. Lett.* **2008**, *18*, 4339−4343.
(36) Akwabi-Ameyaw, A.; Caravella, J. A.; Chen, L.; Creech, K. L.; Deaton, D. N.; Madauss, K. P.; Marr, H. B.; Miller, A. B.; Navas, F.; Parks, D. J.; Spearing, P. K.; Todd, D.; Williams, S. P.; Wisely, G. B. Conformationally constrained farnesoid X receptor (FXR) agonists: alternative replacements of the stilbene. *Bioorg. Med. Chem. Lett.* **2011**, *21*, 6154−6160.